Discrimination of Agricultural Crop Types Using a Spectral-Spatial Unmixing Approach

Master's Thesis by Jonas E. Böhler

GEO 511 Master's Thesis

Discrimination of Agricultural Crop Types Using a Spectral-Spatial Unmixing Approach

Jonas E. Böhler

Matriculation Number: 05-913-124

April 30th, 2014

Adviser: Dr. Mathias Kneubühler

Faculty Representative: Prof. Dr. Michael E. Schaepman

Acknowledgments

I would like to thank a number of people for contributing to the success of my master's thesis. First and most important of all, I would like to thank my wife and my son for their patience and understanding during the last months. Special thanks also go to my whole family: It was possible to find enough time for my thesis at the end only through the countless days of child care for my son by the whole family.

Thanks go to various people at the RSL: Mathias Kneubühler always had time for my questions and provided important inputs to problems from creating the first draft to the completion of the thesis. Michael E. Schaepman made it possible for me to write the thesis at the RSL and provided project support. Daniela Braun processed the data several times for me and was a great help in any R challenges. I would like to thank the whole RSL staff, Daniel Kükenbrink and Christoph Rohner for the varied breaks and inputs of any kind.

Special thanks go to Jörg Weyermann for his great effort in correcting the whole thesis and Martina Flick and Samuel Witzig for linguistic and formal corrections. As usual, all remaining errors are my responsibility.

Abstract

Remote sensing is an important instrument in land cover classification and precision agriculture. The considerable progresses in imaging spectroscopy during the past years now allow spectral mixture analysis at the subpixel level. This enables to determine the adequate distribution of different crop types in a single field.

A main problem in mixture analysis is the spectral and spatial variation of vegetation signatures. This fact is often neglected in conventional approaches based on linear spectral analysis. To account for the spatial relationship, a new method is proposed that uses the variogram and determines the abundances based on Bayes' theorem. The method is applied on a reduced imaging spectroscopy data set acquired by the airborne prism experiment (APEX) instrument on May 14th, 2013. A agricultural test site of 10 km^2 near Lyss (BE) in the Swiss midlands is used to determine the abundances of ten crop types and to calculate a classification based on the highest abundances. The classification of the proposed method reaches an overall accuracy of 54.45% and a kappa coefficient of 0.08.

The results are compared to a conventional approach based on pixel purity index derived endmembers and linear spectral unmixing. The conventional approach reaches an overall accuracy of 23.4% for the classification with the highest abundances. There is a mean R^2 of 0.045 for the abundances of the crop types between the proposed method and conventional approach.

There are several reasons for these low values with the new method and the conventional approach of the accuracy indicators. First of all, it is difficult to differentiate agricultural plants in this early stage of development. Furthermore, the results of the conventional approach have restricted validity, since there are linear dependencies for endmembers and therefore no unique linear spectral unmixing is possible. The proposed method calculates small abundances for the majority of the pixels for each of the ten crop types. Consequently it is more appropriate to use this method to express a membership of crop type at a pixel level rather than to calculate exact fractions at the pixel area.

Zusammenfassung

Fernerkundung ist ein wichtiges Instrument für Landnutzungsklassifikationen und/oder Precision Farming. In den vergangenen Jahrzehnten wurden beträchtliche Fortschritte im Bereich der abbildenden Spektroskopie gemacht, die es ermöglichen, die spektrale Mischung im Subpixelbereich zu analysieren. Dies erlaubt die adäquate Verteilung von verschiedenen Feldfrüchten in einem Feld zu bestimmen.

Ein Hauptproblem in der Analyse von gemischten Pixeln ist die spektrale und räumliche Variabilität von Pflanzensignaturen. Diese Tatsache wird in den herkömmlichen, auf linearen Spektralanalysen basierenden Ansätzen oft vernachlässigt. Um die räumlichen Zusammenhängen zu berücksichtigen, wird eine neue Methode vorgeschlagen, welche mittels Variogramberechnungen und basierend auf dem Theorem von Bayes die Anteile eines Feldtyps in einem Pixel ermittelt. Die Methode wird auf reduzierte abbildende Spektroskopiedaten, die vom «airborne prism experiment» (APEX) Instrument am 14. May 2013 aufgenommen wurden, angewendet. Im 10 km^2 grossen Testgebiet in der Nähe von Lyss (BE) im schweizerischen Mittelland werden die Anteile von zehn verschiedenen Feldfrüchten bestimmt und anhand der höchsten Anteile an einem Pixel klassiert. Mit der vorgeschlagenen Methode wird eine Gesamtgenauigkeit von 54.45% und ein Kappa Koeffizient von 0.08 erreicht.

Die Resultate werden mit einem herkömmlichen Ansatz verglichen, der die Pixelsignaturen mittels «pixel purity index» bestimmter «endmember» linear entmischt. Dieser Ansatz erreicht eine Gesamtgenauigkeit von 23.4% für die Klassifikation der höchsten Anteile. Der durchschnittliche R^2-Wert zwischen der vorgeschlagenen Methode und dem herkömmlichen Ansatz für die zehn Feldtypen beträgt 0.045.

Es gibt verschiedene Gründe für die tiefen Genauigkeitsindikatoren der vorgeschlagenen Methode und dem herkömmlichen Ansatz. Zuerst muss erwähnt werden, dass eine Unterscheidung von Feldfrüchten in diesem frühen Entwicklungsstadium schwierig ist. Ausserdem haben die Resultate des herkömmlichen Ansatzes nur beschränkte Gültigkeit, da die «endmember» linear abhängig sind und daher keine eindeutige lineare Entmischung möglich ist. Die vorgeschlagene Methode berechnet für die Mehrheit der Pixel kleine Anteile für alle zehn Feldtypen. Folglich ist es eher angemessen, die Resultate als Zugehörigkeit zu einem Pixel aufzufassen denn als exakte Flächenanteile an einem Pixel.

Contents

List of Figures

List of Tables

1. Introduction

1.1. Motivation

Remote sensing is an important tool in land cover or land use classification and in precision agriculture (Villa et al., 2011). Information on agricultural land use is often available only on administrative units or statistics on regional or national scales (De Wit and Clevers, 2004). However, there are many agro-environmental applications that need information on the field level, i.e. assessment of flood damage or water quality (Foerster et al., 2012). Remote sensing data are further relevant in precision farming (Mulla, 2013), an important step forward in agricultural controlling and monitoring (Crookston, 2006).

Multispectral satellite imagery has been used for land use classifications since the 1970s. In Midwestern US agricultural landscapes have been classified in corn and soybean fields with an overall accuracy (OA) of 83% (Bauer and Cipra, 1973). With several data sets from various recording times cereal crops, field crops, grassland and forest land have been classified with an OA of 88% in East Anglia, UK (Jewell, 1989) and rice and potato cropping systems with an OA of 95% in India (Panigrahy and Chakraborty, 1998).

Considerable progress has been made in imaging spectroscopy (IS) technology for remote sensing applications in the last decades (Keshava and Mustard, 2002). A high spatial and spectral resolution can be achieved at the same data acquisition (Bioucas-Dias et al., 2013; Keshava and Mustard, 2002). IS data sets have the advantage that it contain information on the fractional composition of a single pixel, whereas multispectral data can be used for classification of the whole pixel. Information of an image is spectrally smooth, i.e. there is a high correlation between neighboring spectral bands, and they are spatially piecewise smooth (Bioucas-Dias et al., 2013). Neighboring pixels often have the same content until they capture another surface phenomenon. A good example is grass, which is spectrally and spatially smooth (at the spatial resolution of common airborne instruments). The content of a pixel changes only at the border to a building (Figure 1.1). Nevertheless, a spatial pixel often represents a combination of different land cover types (Villa et al., 2011).

To account for this fact, soft classification approaches are used: They do not assign a single class to a pixel, but calculate the membership of a pixel to a class (Nachtegael et al., 2007). This membership corresponds not necessarily to surface fractions only (Villa et al., 2011). Linear spectral mixture analysis (SMA) addresses this problem: Classes are called endmembers, the membership is called abundance. Only few and clearly distinguishable classes like soil, grass and bedrock (Mustard, 1993) or green vegetation, shade and soil (Roberts et al., 1993) are typically used. Wang et al. (2007) unmixed four highly mixed plant types and soil in salt marshes. SMA is used in agriculture for crop residue determination (Bannari et al., 2006; Pacheco and McNairn,

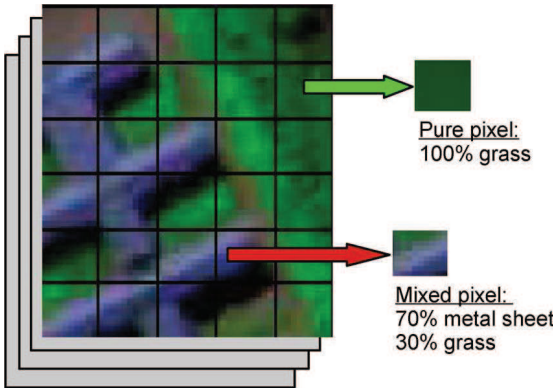

Figure 1.1.: Mixture between different land cover types (Villa et al., 2011).

2010) or improved biophysical parameters estimation (Peddle and Smith, 2005). For the validation of the results, they use R^2 or root-mean-square error (RMSE) between unmixing results and ground truth.

A main problem of linear SMA is the spatial and spectral variation of an endmember (Somers et al., 2011). The algorithms used for the works mentioned above do not entirely use the spatial relation between the observed spectra and neglect the spectral variability of an endmember. To get these two sources of information into the mixture model, a variogram based method is proposed in this thesis. The mixture is then calculated based on Bayes' theorem.

1.2. Objectives and Outline

The underlying objective of this thesis is to answer the following main research question:

Is it possible to capture the endmember variation of crop plants in an early stage of development for a mixture analysis by the proposed method?

In other words, the possibility to distinguish between different crop types in a data set of an agricultural field scene will be analyzed. A single data set of May 2013 and ground truth data of June 2013 are used. Since no additional data for validation is available, an accuracy assessment with a hard classification will be done and the abundance results will be compared to a linear spectral unmixing (LSU) with pixel purity index (PPI) derived endmembers.

Derived from the main objective above, this thesis treats the following subordinate research questions:

1. Are there spectral differences between crop plants in an early stage of development?

2. Can the chosen proposed method explain the mixture in a pixel?

3. Is the proposed method more suitable for classification?

4. How does the proposed method perform compared to a conventional approach based on PPI and LSU?

This thesis is structured into six main chapters. After this introduction follows the description of the study site in the second chapter. The methods used for the spectral spatial approach and the PPI are described in the third chapter. The results of these two methods are described and discussed in the fourth and fifth chapter. The synthesis and an outlook are discussed in the final chapter.

2. Data

2.1. Test site

The test site is located near Lyss in the Bernese Lakeland in the Swiss midland (Figure 2.1a) at 585 267 to 587 795 N and 212 200 to 216 230 E (Swiss coordinate system, CH1903) 460-477 m above sea level (a.s.l.). This agricultural area is split up in small fields from 150 m^2 to 55000 m^2 and crossed by farm tracks and streets which connect small surrounding towns (Figure 2.1b).

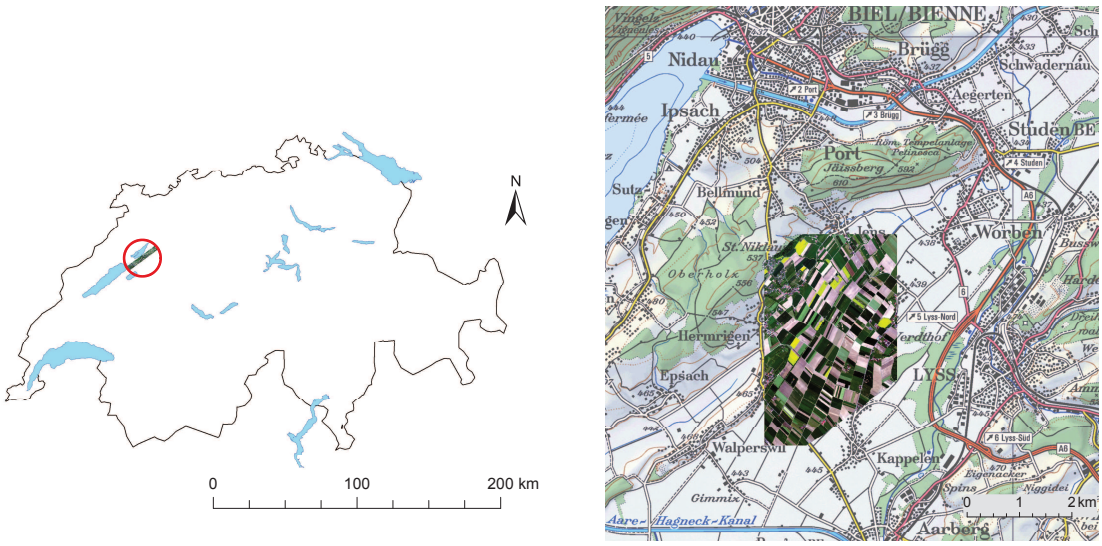

(a) (b)

Figure 2.1.: (a) Location of the test site in Switzerland and APEX flight stripe (red circle). (b) Subset of the test site over map. (Source: Bundesamt für Landestopografie)

2.2. Imaging Spectrometer Data

IS data of the airborne prism experiment (APEX) instrument is used for this thesis, recorded on May 14th 2013. The spectral range of the visible and near-infrared (VNIR) and short-wavelength infrared (SWIR) detectors ranges from 375 to 2500 nm and offers up to 532 spectrally continuous bands. The spectral bands have been resampled in pre-processing to 299 channels. Ground pixel sizes of 1.5-2.5 m result at typical flight altitudes of 3000-5000 m above ground with a field of view of 28° (Hueni et al., 2013). The flying altitude of the data used in this thesis was 3500 m above ground with a

resulting ground pixel size of 2 m after atmospheric and geometric (nearest neighbor) correction.

Detailed ground truth was acquired in the test area on June 26th 2013. 299 agricultural fields have been classified in 10 classes. All classes and the number of fields for each class can be found in Table 2.1. A region of interest (ROI) was manually built for each field to receive training and control data. The boundary pixels of each field and disturbing objects such as power line or bare soil patches were excluded if possible to avoid mixed pixels (Figure 2.2).

Due to the time gap between the APEX overflight and ground truth data acquisition, not all the crop plants mapped on June 26th could be traced back to the May 14th APEX scene. E.g. fields with corn in June have been planted on fields that were bare soil or meadow in May. It appears that there are two different types of meadow fields, probably perennials (Figure 2.3a) and annual (Figure 2.3b). The perennials have been classified as *meadow*, the annuals as *meadow young* based on visual criteria. Most of the *meadow young* fields had been planted with corn between May and June. Because there is only one *sugar pea* field in the study site, this field is divided up in a two-third and one-third part for training and control. Some misclassifications are possible, caused by the time-lag. Two classes were defined for bare soil: Some bare soil fields in the scene are obviously brighter than others, probably caused by a number of factors such as water content, time of plowing or composition of organic material. Although the reason for this difference is unclear, two classes (*bare soil* and *bare soil bright*) have been defined due to optical appearance.

Table 2.1.: Crop types, their scientific name and corresponding number of training and control fields

crop type	scientific name	number of fields		
		total	training	control
alfalfa	Medicago sativa L.	3	2	1
bare soil	-	56	38	18
bare soil bright	-	50	33	17
meadow	-	50	33	17
meadow young	-	26	16	7
rapeseed	Brassica napus L.	16	11	5
spring barley	Hordeum vulgare L.	21	14	7
sugar pea	Pisum sativum L. convar. axiphium Alef.	1	2/3	1/3
winter barley	Hordeum vulgare L.	17	12	5
winter wheat	Triticum L.	62	41	21

As the measurement and the ground truth did not take place on the same date, the phenological stage of the plant can only be estimated. Spring 2013 was colder and the vegetation was developing later than usual (MeteoSchweiz, 2013a). The warmest temperatures were measured at the beginning of May. The middle third of May was cool and had a low sunshine duration and on 21 May the winter returned. The very cool and wet weather held up partially until 26 May. The vegetation development was locally different and varied depending on plant type plus or minus one week to the

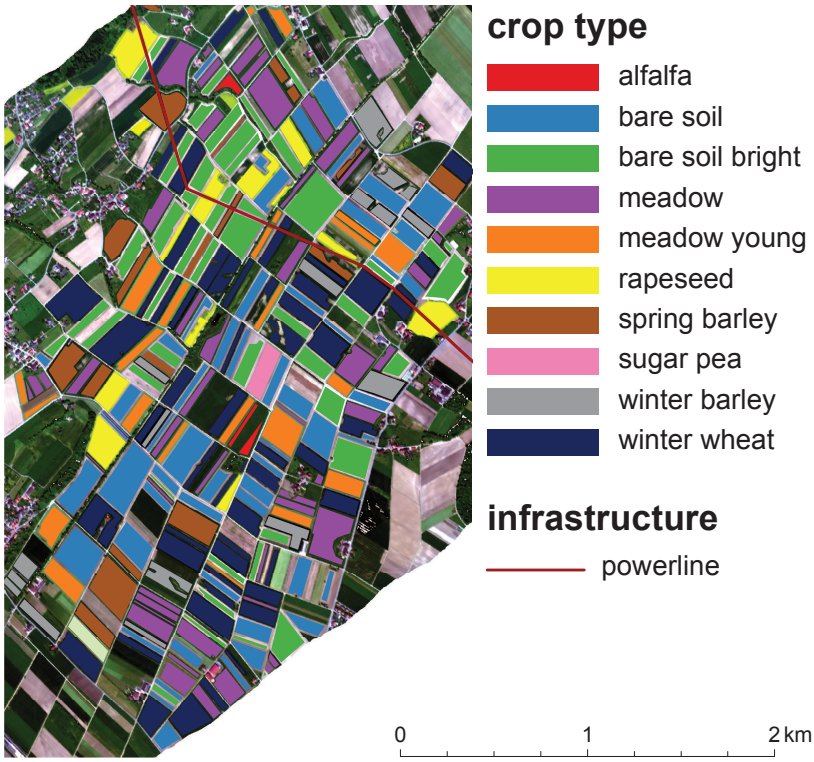

Figure 2.2.: Ground truth and infrastructure on true color image of the APEX scene.

average of 1980 to 2010. Due to the fact that May was comparably cold and wet, the vegetation in the lowlands showed a rather late development (MeteoSchweiz, 2013b).

For the description of the growth stage of crops and weed the «Biologische Bundesanstalt, Bundessortenamt und Chemische Industrie» (BBCH) scale (Lancashire et al., 1991) can be used. This is used in a remote sensing topic for example by Torres-Sánchez et al. (2014). The best information about the phenological stage can be found for rapeseed, which is mostly in a stage of flowering (stage 6). However, there are still some green parts which are inflorescence emergence (stage 5) in the classification of BBCH (Figure 2.4). For other crop types, a classification was not possible afterward. It seems that the fields were sometimes very wet and some winter barley and wheat fields were partially sown in another time (Figure 2.5).

In this early stage of the plant growth, the different types are spectrally very similar. This could already be seen in the mean spectra of the different crop types (Figure 2.6a). For improved comparability, the continuum removed values are calculated (Clark and Roush, 1984). The similarity of the spectra of *bare soil*, *bare soil bright* and *sugar pea* is already noticeable in the mean spectra and clearly in the continuum removed spectra (Figure 2.6b). The signature of these curves is partially congruent. Only *sugar pea* has some bigger differences in the blue and red part of the spectrum. It seems that the *sugar pea* cover is very small in May and most of the reflectance originates from the ground. The signatures of the other crop types show the typical vegetation signature. The three crop types and two meadow types have a similar spectral signature. Only *meadow young* and *rapeseed* could be distinguished from the other vegetation spectra

(a) (b)

Figure 2.3.: Pictures of the two meadow types *meadow* (perennials meadow) (a) and *meadow young* (annual meadow) (b) (recording from June 26th, 2013).

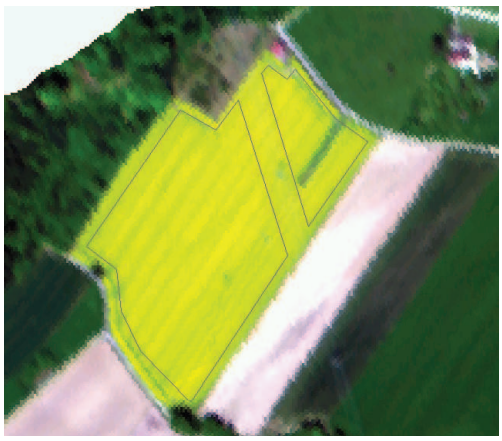

Figure 2.4.: *Rapeseed* field in BBCH stage 5 (green) and 6 (yellow) at acquisition on May 14th, 2013. The black polygon marks the ROI which is divided into two parts by the exclusion of the power line. The field is locatet in the north of the test site at (585 970/216 000).

in the green part of the spectrum.

Figure 2.5.: A *spring wheat* stripe that is sown later in a *winter wheat* field (recording from June 26th, 2013).

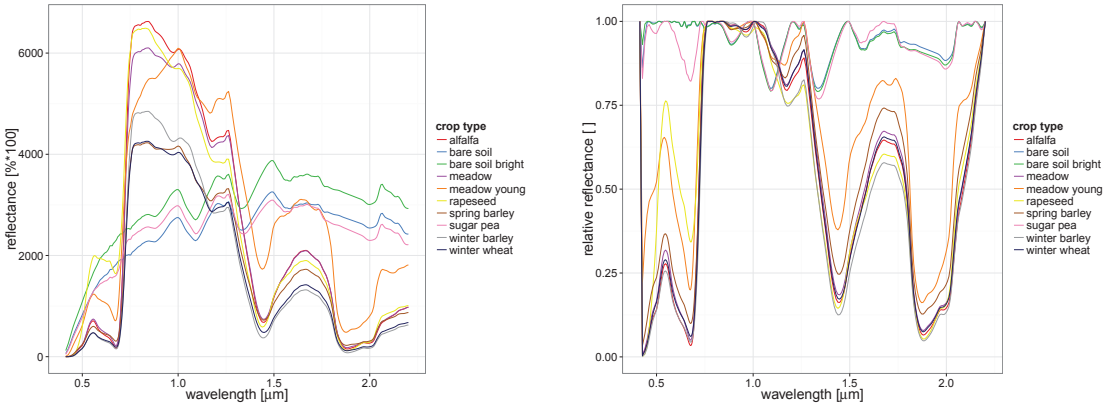

(a) (b)

Figure 2.6.: Mean spectra of the ROIs of each crop type (a) and continuum removed mean spectra (b).

3. Methods

This chapter is structured into two parts. The theoretical background is explained first, the proposed method and the conventional approach based on PPI and LSU is presented in the second part.

3.1. Theoretical Background

3.1.1. Spectral Mixture Analysis

Mixed pixels always occur in remote sensing data sets, as mentioned in the introduction. There are two reasons for mixed pixels: the spatial resolution of the sensor is not high enough or the land cover consists of a homogeneous (intimate) mixture of different materials (Keshava and Mustard, 2002). The former is caused by the given sensor resolution and the flying altitude of the sensor system over ground. The latter is independent of sensor parameters and caused by light interacts with multiple materials (Plaza et al., 2004).

Spectral unmixing is a process of splitting the spectrum of a mixed pixel into its constituent spectra or spectral signatures, called endmembers (Keshava and Mustard, 2002; Bioucas-Dias et al., 2012). Each endmember has its own fraction or abundance, describing its percentage within the respective pixel. An endmember represents the pure material which occurs in the data set such as soil, vegetation or forest. Spectral unmixing is an inverse problem which is ill-posed when not all endmembers are known (Bioucas-Dias et al., 2012).

The main problem of the definitions of endmember and abundance is the ambiguity of a pure endmember (Bioucas-Dias et al., 2012). It is a question of the objectives of an application. For example, if simple discrimination between vegetation, soil and water is necessary, the whole vegetation can be treated as a single endmember. Vegetation however consists not only of one ingredient. It is a community of diverse plants such as trees and herbage. One can further differentiate between families, subfamilies and so on. Another differentiation into leafs, trunk, flowers, and so on is possible. On the other hand, the meaning of abundances is also ambiguous (Bioucas-Dias et al., 2012). The assumption that the abundance corresponds to the area covered by an endmember in a pixel holds true only in the linear case. For nonlinear settings, laboratory experiments have shown that it is not necessary true (Bioucas-Dias et al., 2012). The percentage of the reflectance is no longer a linear function of the area involved, but rather a volume of an object or a small, highly reflective object can dominate a dark object in a reflected spectrum of a pixel.

As mentioned above, there are two kinds of mixture: linear or nonlinear (Figure 3.1). Linear mixture occurs in checkerboard scenes where the endmembers occur in spatially separated patterns (Keshava and Mustard, 2002). Hence there is no interaction between endmembers and only one material interacts with the incoming light. The linear mixing

is therefore on a macroscopic scale and is a consequence of the large spatial resolution (Keshava and Mustard, 2002; Bioucas-Dias et al., 2013). The mixture happens therefore in the sensor itself (Bioucas-Dias et al., 2012).

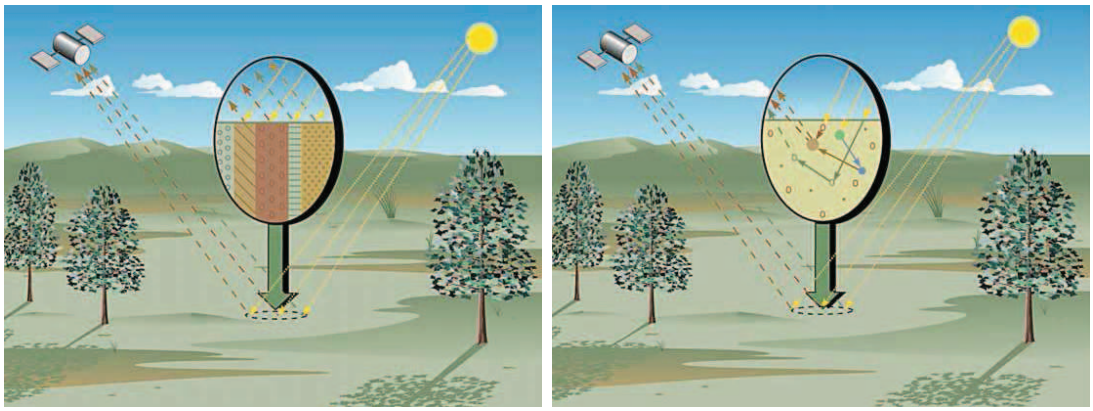

(a) (b)

Figure 3.1.: Illustration of the two basic kinds of mixture: linear mixing of a checkerboard surface (a) and nonlinear mixing of multiple scattering (b) (Keshava and Mustard, 2002).

The other kind of mixture model is nonlinear and a physical consequence of the interaction between two (or more) endmembers. There are two types of nonlinear mixture (Figure 3.2). In the first type, the mixture occurs at a microscopic or intimate scale (Figure 3.2a), in which photons are emitted by a molecule of one substance, and are absorbed by another and vice versa (Bioucas-Dias et al., 2012; Keshava and Mustard, 2002). In the second type, the mixture can occur by multiple scattering between two or more layers (Figure 3.2b). This is typically the case in vegetation scenes where the incoming light is reflected by ground to canopy, canopy to ground, canopy to canopy, etc. and in the end to the sensor. It is easy to imagine that there are a lot of possible reflections, especially for more than two layers, i.e. at leaf level. Both nonlinear mixture processes occur outside the sensor in contrast to the linear case (Bioucas-Dias et al., 2013).

3.1.2. Linear Mixing Model

Due to its simplicity, the linear mixing model (LMM) has been frequently used in the last decades. Two further reasons are the acceptable approximation and the fact that it is a well-posed inverse problem under suitable conditions (Bioucas-Dias et al., 2013). The inversion of a LMM is called LSU and is used in the conventional approach. The measured vector is $y := [y_1, \ldots, y_n]^\intercal$ where y_i is the data value in band i and n is the number of bands in the data cube. The resulting vector can be expressed as a linear combination of endmembers m_i:

$$y = \sum_{i=1}^{p} \alpha_i m_i \tag{3.1}$$

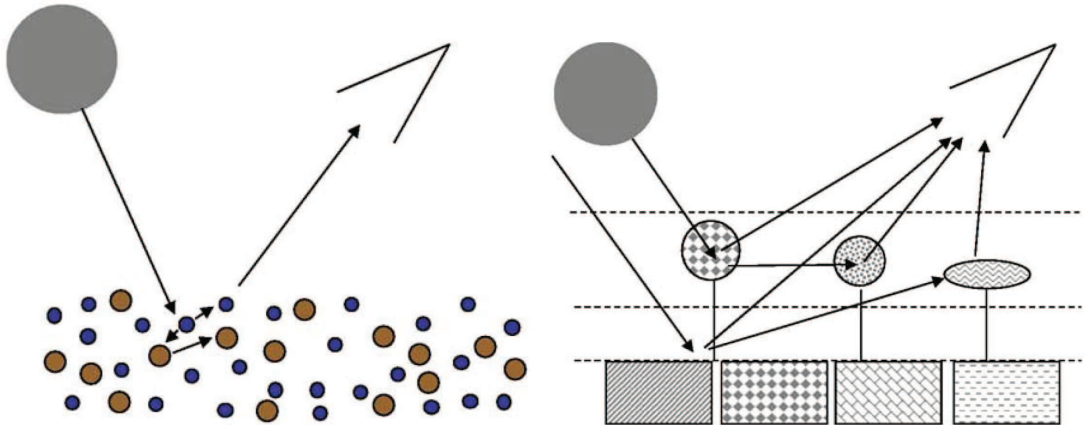

(a) (b)

Figure 3.2.: Illustration of the two kinds of nonlinear mixture: intimate mixture (a) and multilayer mixture (b), here two layer of canopies and ground (Bioucas-Dias et al., 2012)

where α_i is the abundance of the endmember m_i with p endmembers (Adams et al., 1986). A visual illustration with three endmembers can be found in Figure 3.3.

There are two physically based constraints for the abundances α_i (Somers et al., 2011). Due to the fact that an endmember m_i can occur or not, negative values for the corresponding fraction α_i make no sense. This is the abundance nonnegativity constraint (ANC)

$$\alpha_i \geq 0 \tag{3.2}$$

for $i = 1, \ldots, p$. The second constraint, the full additive condition or abundance sum-to-one constraint (ASC), proposes that the whole pixel value can be explained by endmembers and therefore holds

$$\sum_{i=1}^{p} \alpha_i = 1 \tag{3.3}$$

Due to the fact that there is some variability in the spectra of an endmember, especially in vegetation scenes, the ASC can rarely be fulfilled in real applications. Given that α_i is positive (ANC holds), the ASC can be fulfilled with a simple rescaling (Bioucas-Dias et al., 2013).

For model mismatches or additive noise, an additive vector w can be added to (3.1) and the equation can be written as

$$y = M\alpha + w \tag{3.4}$$

where $M := [m_1, \ldots, m_p]$ is the mixing matrix and $\alpha := [\alpha_1, \ldots, \alpha_p]^\intercal$is the abundance vector. The observed spectral vectors y can be considered as points in a n-dimensional space. This point cloud can be enveloped by a convex hull $C = conv\{M\}$, the so called simplex (Figure 3.4) (Nascimento and Bioucas-Dias, 2005).

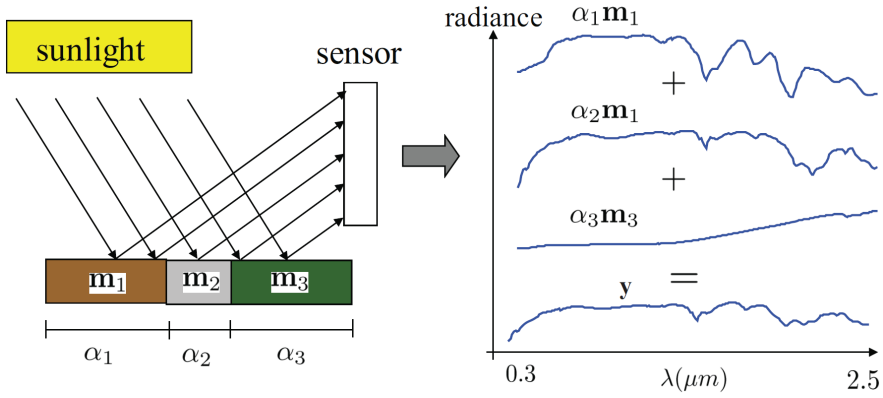

Figure 3.3.: Measured pixel value y as linear mixture of three endmembers (Bioucas-Dias and Plaza, 2010).

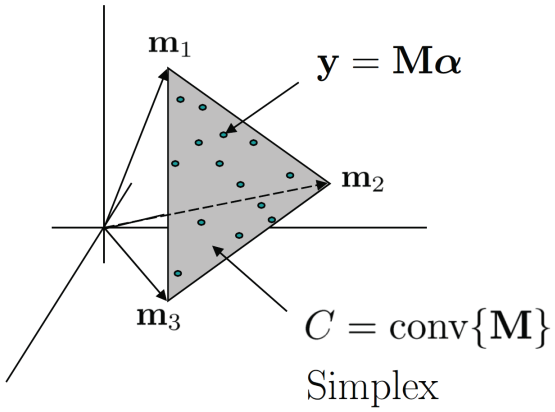

Figure 3.4.: Two dimensional simplex for three endmembers. The green points symbolize observed vectors. Red points symbolize the vertex and correspond in this case to endmembers (Bioucas-Dias and Plaza, 2010).

3.1.3. Unmixing imaging spectroscopy data

The processing chain for an unmixing task contains several steps (Figure 3.5). In a first step, the radiance data from the IS data sensor have to be adjusted atmospherically and, if needed, geometrically. The atmospheric correction removes scattering effects of the atmosphere (Bioucas-Dias and Plaza, 2010). The resulting reflectance values describe inherent properties of the surface and are independent of illumination characteristics (Bioucas-Dias and Plaza, 2010). The LMM can be applied with radiance data as well (Keshava and Mustard, 2002). A geometric correction is required if a comparison with independent geo-located data like a ground truth is part of the application. Since large parts of the information in reflectance (or radiance) data are redundant, a dimension reduction decreases the computational effort (Bioucas-Dias and Plaza, 2010). This is again not a necessary step for an unmixing task. In a last step the unmixing itself can be realized. This can be done by endmember determination and the inversion of the LMM, sparse coding (Olshausen and Field, 1996) or sparse regression (Iordache et al., 2011). An inversion has the ambition to minimize the error term (Van der Meer, 1999). The

main problem of the inversion algorithms is to fulfill the ASC and ANC. The majority of the algorithms try to minimize the least squared error (Keshava and Mustard, 2002). The error image explains parts of missing or incorrect endmembers.

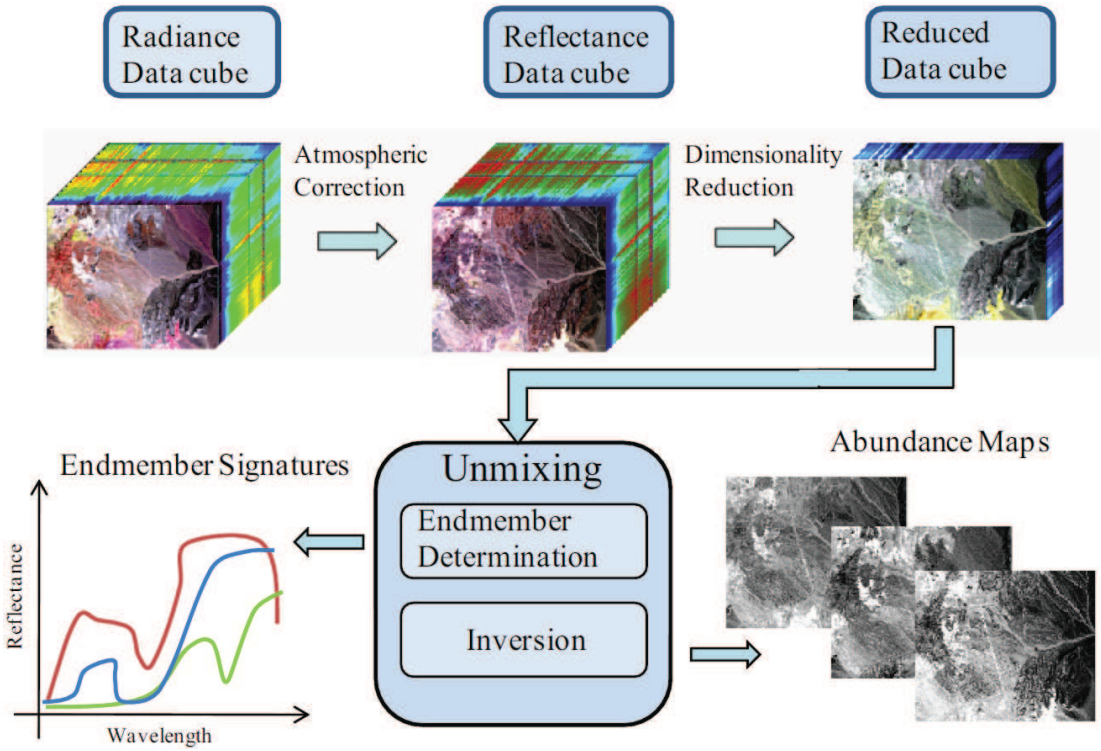

Figure 3.5.: Processing chain of unmixing for IS data (Bioucas-Dias and Plaza, 2010).

3.1.3.1. Dimension reduction

The objective of the dimension reduction is the generation of a data set without redundant information. This decreases the computation time and complexity and increase the signal-to-noise-ratio (SNR) (Bioucas-Dias and Plaza, 2010). Minimized storage space is an appreciated side effect. A first step is the selection of bands. This allows to use a subset of original data with the advantage of preserving original information (Chang and Wang, 2006).

Several algorithms exist that search for new projections to reduce the dimensions in a data space. Principal component analysis (PCA) searches for new orthogonal axis in the data space with maximum variance. This is achieved by an eigendecomposition (Jolliffe, 2005). The minimum noise fraction (MNF) transformation works similar to the PCA, but takes also the SNR into account (Green et al., 1988). The MNF is a mathematical equivalent with the noise adjusted principle components (NAPC) (Lee et al., 1990). PCA is the best algorithm in least square sense for the data and MNF/NAPC is optimal for the ratio of noise power to signal power (Bioucas-Dias and Plaza, 2010). In addition to these two frequently used concepts, there exists a third one based on singular value decomposition (SVD) (Scharf, 1991), which completes the collection with the most efficient algorithm in maximum power sense (Bioucas-Dias and Plaza, 2010).

3.1.3.2. Endmember Selection

Endmember selection can be divided into three types of methods: pure pixel based, non-pure pixel based, and statistical algorithms (Bioucas-Dias et al., 2013). Pure pixel based algorithms assume that at least one pure pixel per endmember can be found in the data. An endmember corresponds then to a vertex of the simplex (Figure 3.4). This is a strong constraint that is not fulfilled for many data sets. PPI (Boardman, 1993) or N-FINDER (Winter, 1999) are two representatives of this group. If there are no pure pixels in the data a minimum volume (MV) approach can be chosen. With such an algorithm endmembers are constructed spanning a MV around the data simplex. The vertex of this volume is chosen as endmember (Craig, 1994). Highly mixed data sets do not contain pure pixels and the MV approach fails as well. However, statistical algorithms can deal with this problem. These algorithms are usually based on Bayes' theorem and the mixing matrix is calculated with Markov chain Monte Carlo algorithms (Bioucas-Dias et al., 2013).

Image-derived endmembers have the advantage of being retrieved under the similar atmospheric conditions as the image data itself (Van der Meer, 1999). They have a physical meaning, because they exist in the real world. However, they are often mixtures of other materials and as a consequence, the resulting abundances do not always fulfill the ANC, even if satisfying the ASC (Keshava and Mustard, 2002). For multitemporal studies or data with different illumination conditions a library of endmember is required. This library could be collected under laboratory conditions as well (Keshava and Mustard, 2002).

All the algorithms mentioned above do not use the spatial relation between the observed spectra and neglect the spectral variability of an endmember. To combine these two sources of information into the mixture model a variogram based approach is used in this thesis. The optimal mixture is then calculated based on Bayes' theorem.

3.1.4. Variogram

Variogram[1] determination includes two steps. In a first step the variogram is calculated, in a second step a theoretical model is fitted to this variogram (Chilès and Delfiner, 2012).

The variogram is defined as half the variance between a measurement at two samples or points with a certain distance, called *lag*. In case of optical remote sensing, the *lag* distance h is the interval between two points on a transect through the image pixels (Figure 3.7) and can be considered as vector with a distance and direction (Curran and Atkinson, 1998). There are multiple point pairs with a certain *lag* distance in remote sensing data sets. A pixel is usually used for the sample size, called *support* in variogram theory. Thus the *lag* distance corresponds to the spatial resolution of the data set. Analysis of half of the squared difference between measurement of point pairs with *lag* distance h apart from each other leads to the variogram cloud (Figure 3.6). The variogram cloud shows the *lag* distance along the horizontal axis and the half squared

[1] There are several terms for variogram: theoretical, experimental, sample or semi- variogram. The abbreviation and simple term «variogram» seems to become established (Atkinson and Lewis, 2000; Chilès and Delfiner, 2012). In this thesis the term variogram will be used.

increment along the vertical axis $\frac{1}{2}[z(x_i) - z(x_{i+h})]^2$, where $z(x_i)$ is the measurement at position x_i, $z(x_{i+h})$ at x_{i+h} (Chilès and Delfiner, 2012).

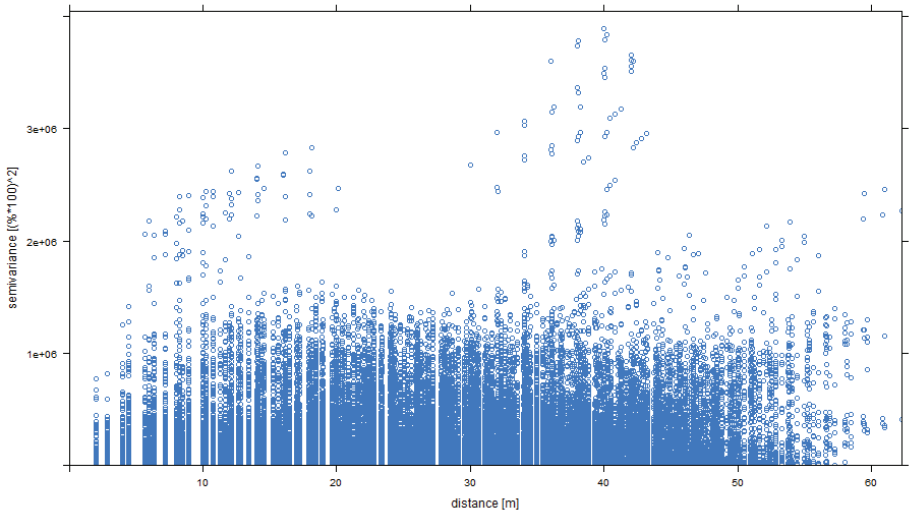

Figure 3.6.: Variogram cloud of a meadow *young* field. Pixel pairs (blue circle) are more similar for low semivariance values.

From the variogram cloud the variogram is given as the mean value of the half squared increment and as function of the *lag* distance h(Chilès and Delfiner, 2012). Therefore, the definition of a variogram $\gamma(h)$ is given by

$$\gamma(h) = \frac{1}{2N(h)} \sum_{i=1}^{N(h)} [z(x_i) - z(x_{i+h})]^2 \tag{3.5}$$

where $N(h)$ is the number of point pairs separated by the *lag* distance h. Under conditions of isotropic phenomenon propagation, the variation is the same in all *lag* directions, whereas under anisotropic conditions[2] this is not the case (Van der Meer, 2012). The variogram expresses the dissimilarity between spatially separated pixels in a useful manner (Jupp et al., 1988). It is essential for further geostatistics to fit a mathematical model to the variogram function (Woodcock et al., 1988).

Several terms exist that describe a variogram model (Figure 3.8 and Table 3.1). *Range* and *sill* are linked in the fashion that the *range* corresponds to the (*lag*) distance at which the *sill* is reached, or vice versa. At distances longer than the *range*, point pairs are not correlated anymore. The *nugget*[3] describes the behavior near the origin and is called *nugget effect*, if it is nonzero due to a discontinuity (Chilès and Delfiner, 2012). As mentioned above, the *support* is the sample size and shape. It is only important if it is not alike for all samples (Chilès and Delfiner, 2012).

For the fitting of a model to a variogram, the three parameters *nugget*, *range* and *sill* are important (Van der Meer, 2012). In remote sensing the exponential (Exp) and

[2]For example, a meadow spreads in all directions equally, so it is isotropic, whereas potatoes are planted in rows with soil in between. This results in an anisotropic propagation.

[3]The concept comes from the gold nugget, which are smaller than the support (Chilès and Delfiner, 2012).

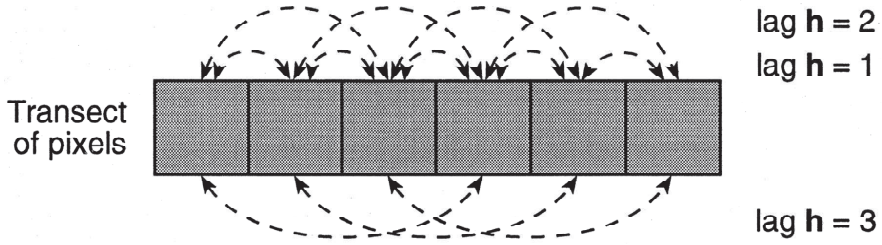

Figure 3.7.: Pixels of a transect with lag distance 1, 2 and 3 (Curran and Atkinson, 1998).

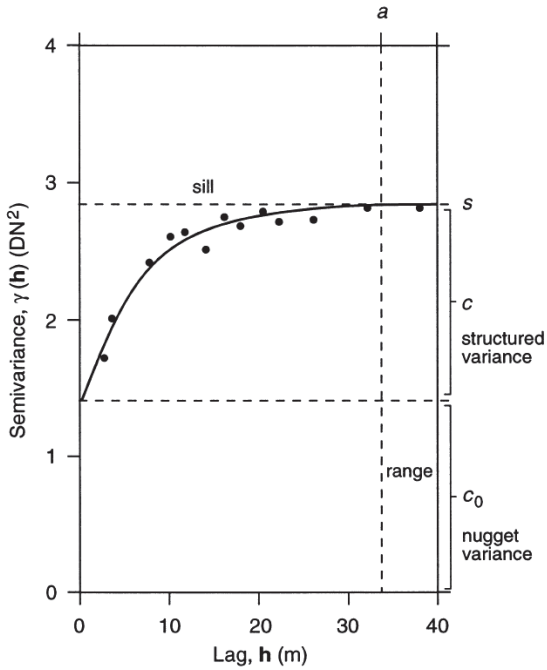

Figure 3.8.: Variogram with fitted model (Curran and Atkinson, 1998).

spherical models (Sph) are popular (Garrigues et al., 2008b). The Sph achieves a well-defined *sill* (Figure 3.9a), whereas the Exp reaches the *sill* only asymptotically (Figure 3.9b). Therefore the so called *practical range* is used. This is usually the distance at which 95% of the *sill* is reached (Chilès and Delfiner, 2012). The normalized variogram model formula describes the structural variance (Table 3.2).

In remote sensing, the variogram is mostly used for estimations of a single value with Kriging algorithms, e.g. soil moisture or biomass (Curran and Atkinson, 1998). In this thesis, the structure of ten different agricultural crop types will be analyzed with a geostatistical mixture approach. Therefore the variance at the range will be used for the conditional probability per class. In the present work the range of the variogram model is used to describe the variation of the endmembers.

Table 3.1.: Terms of variogram description (Curran and Atkinson, 1998; Van der Meer, 2012).

Term	Symbol	Definition
Support	y	Shape and size of a sample
Lag	h	Interval between two points (vector with distance and direction)
Sill	s	Maximum value of the fitted variogram model where the range is reached
Range	a	Distance where the sill is reached
Nugget variance	c_0	non-zero y-intercept (short term nugget)
Structured variance	c	Sill minus nugget variance

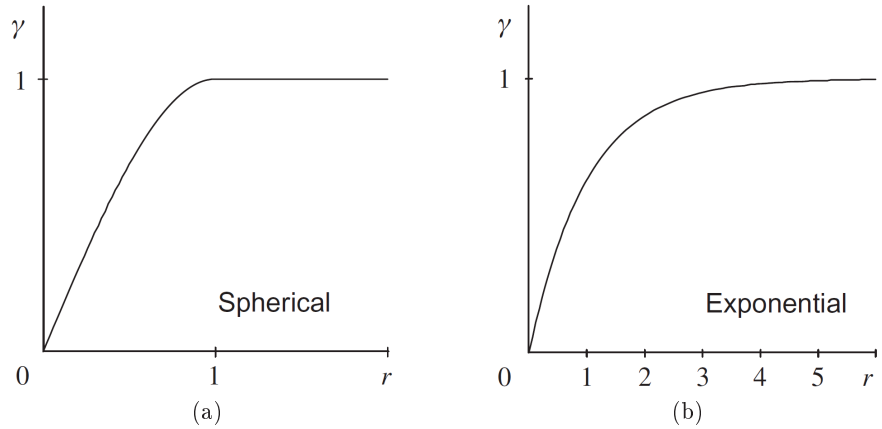

Figure 3.9.: Normalized variogram models of spherical (a) and exponential model (b).

3.2. Proposed Method

To calculate the abundance map of each crop type the following work flow was chosen. In a first step the data was reduced by a PCA. The data set was split up by crop type and a variogram model was fitted to the data of each crop type and PCA band. These models were used to define a threshold value and together with the mean value of each crop type to calculate the abundance with a Bayesian based approach. Finally a classification was made. The following sections describe the method in more detail.

3.2.1. Data Reduction

The data was transformed by a PCA (Richards and Xiuping, 1999) to reduce the computational load. The forward transformation was calculated based on the covariance matrix, the commonly used MNF showed some unexplainable stripes with increased values in the first spectral bands. The same problem was present with the PCA, but not already in the first bands. To overcome this problem two strategies were chosen. In a first step the spectral range was reduced. It seems that the SWIR part of the spectrum somehow caused this pattern. The removal of the first 3 bands which contain almost

Table 3.2.: Normalized spherical and exponential variogram model with lag distance h and range a in case of Sph, practical range in case of Exp respectively.

Model	Formula
Spherical (Sph)	$c = \begin{cases} 1 - \frac{3h}{2a} + \frac{1}{2}\frac{h^3}{a^3} & \text{if } h \leq a \\ 0 & \text{if } a \geq h \end{cases}$
Exponential (Exp)	$exp(-\frac{h}{a})$

no information (all values are near zero in the scene) and the last 10 noisy bands led to improved PCA results. A further reduction improved the result as well, the reasons for which are unclear. A spectral range of 413.6-2201.8 nm (APEX band 4-253) was chosen in the end. With the reduced spectral range, the arbitrary pattern is visible from band 6 and very obvious from band 8 on.

In a second step the number of PCA bands was selected. Usually the sharp bend in the eigenvalue curve is used. In the present case the bend was located at band 3. The eigenvalue for band 4 was larger than 1%, for band 7 0.1% and for band 13 0.01% of the eigenvalue of band 1 (Table 3.3). Because there are spatial patterns visible from band 8 on, a selection of 13 bands could potentially lead to a problem. A second selection criterion was the error defined as the difference between the original and the inverse transformed subset of the inverse transformed signal (based on the covariance matrix again). This is less than 2% compared to the original one for all subsets, which is in the uncertainty range of atmospheric correction and APEX labor calibration (Schaepman et al., submitted). To have as much information as possible in the reduced data set, a subset with 7 PCA bands was selected. With 7 bands, the error of the inverse transformed signal is less than 1.5% and the total computational load was reduced by 97.7% (for more details see Appendix A).

3.2.2. Threshold Value

As shown in Table 2.1, two-thirds of the fields in each class were selected as training and one-third as control data. The PCA data was split up by ROI in training and control fields of each class. The variogram for each crop type and PCA band was calculated and a Sph was fitted in R with the gstat package (Pebesma, 2004). At large distance variogram values do not have an objective physical meaning (Chilès and Delfiner, 2012), therefore variograms are calculated at a maximum distance of two-third (Garrigues et al., 2008a) or the half (Garrigues et al., 2008b) of the extent of the data set. Since there is no clear value in the literature, the default cutoff value by the R-function of one-third of the diagonal distance of the minimum bounding box was chosen for this thesis (Figure 3.10). For a faster calculation of the variogram, the point pairs within the cutoff distance were concentrated in 40 groups. The number of groups is an empirical value and a trade-off between precision and computational load. The model fitting was done by minimizing the ordinary least-squares residuals (Pebesma, 2004).

The sill of the variogram model was used as a threshold value. Since the Sph results in a unique value, this model was selected. There is no nugget effect because the land surface does not change at subpixel level and the crop plants have a more or less regular

Table 3.3.: PCA band and corresponding eigenvalue for the selection by probability criteria.

PCA band	Eigenvalue	%
1	231743215.7	100.000
2	141050158.4	60.865
3	6364576.847	2.746
4	*3719287.829*	*1.605*
5	1727576.371	0.745
6	406742.2688	0.176
7	*247950.4748*	*0.107*
8	181544.1512	0.078
9	103066.8846	0.044
10	60669.52203	0.026
11	43574.15783	0.019
12	32754.32074	0.014
13	*24786.24244*	*0.011*
14	19825.9807	0.009

distribution in the field itself (Garrigues et al., 2008b; Chilès and Delfiner, 2012).

Since the sill is a variance value that defines a spectral distance between two points, an initial value for each band was needed. SMA offers the endmember as purest point. In our case the most representing point is required. Selecting the most similar point in the variogram led to excessive computational load. Therefore the mean value was selected as initial value, as suggested by Atkinson and Lewis (2000). The difference between the mean of all points and the mean value of the most similar points in the variogram cloud was calculated for the *alfalfa* fields and was negligible[4]. The resulting threshold values are shown in Figure 3.11.

3.2.3. Abundance

The abundance $p(c \mid z)$ of a crop type c in a pixel with PCA value z was calculated with a Bayesian based approach:

$$p(c \mid z) = \frac{p(z \mid c)}{\sum_{r=1}^{10} p(z \mid r)} \tag{3.6}$$

where $p(z \mid c)$ is the conditional probability of z given c and all ten crop types r (Atkinson and Lewis, 2000). The conditional probabilities on the right site of the Equation 3.6 were replaced by a band wise univariate distribution. If the pixel value lies within the threshold around the mean value of a crop type, the probability of having this type in the pixel is 1, otherwise 0 for a PCA band. Mathematically this corresponds

[4]That is not surprising since the ROIs of the crops are designed to contain only similar values.

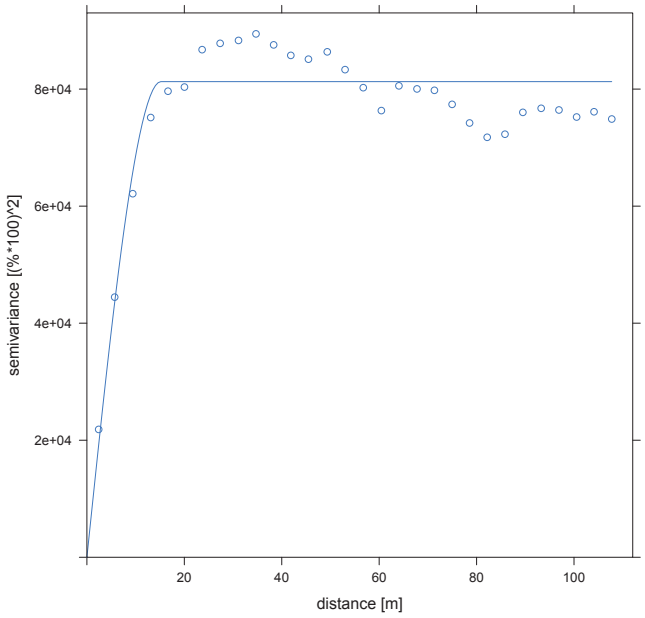

Figure 3.10.: Spherical model fit of the variogram of *alfalfa* in PCA band 4.

to a uniform distribution with the following probability density function

$$f(x) = \begin{cases} 1 & \text{for } t_{min} \leq x \leq t_{max} \\ 0 & \text{otherwise} \end{cases} \tag{3.7}$$

where $t_{min} = mean - threshold\,value$ and $t_{max} = mean + threshold\,value$. The probability density function was calculated for all PCA bands and crop types.

$p(c \mid z)$ is a measure of similarity of a crop type to a pixel and corresponds to the abundance. Through the calculation with (3.6) this value satisfies the ANC and ASC, holding true

$$p(z \mid c) \geq 0 \; \forall c \tag{3.8}$$

and

$$\sum_{s=1}^{10} p(s \mid z) = 1 \tag{3.9}$$

where s are the ten crop types. (3.8) proves the ANC, since the term under the fraction stroke of (3.6) is positive, too. The same denominator effects a normalization to one, therefore holds (3.9) and the ASC. It follows that there is no need for an error image as in the in the LSU.

3.2.4. Classification

The crop type with the highest abundance was selected for the classification, as suggested by Atkinson and Lewis (2000). There are pixels with more than one crop type with the same highest abundance, which offers selection options. A simple method is to select one of the crop types randomly. This is the default behavior of the applied R

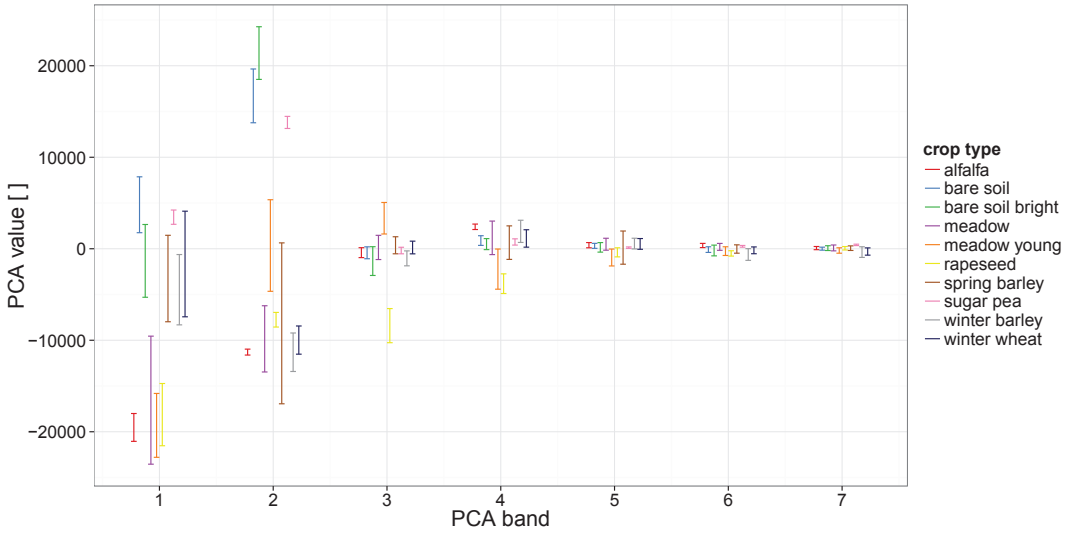

Figure 3.11.: Threshold values of the crop types at the 7 PCA bands.

functions. A more advanced method is to set these pixels to «NA», the «not applicable (NA)» value in R. This makes it possible that no choice has to been made.

In a second step a modal filter was used to smooth the classification result. Especially in the case of the second method this was essential to fill the «holes» with NA in the classification image. In both cases the results is smoothed afterward. For the modal filter different window sizes from 3 up to 29 pixels were used. A window size of 3 pixels takes only the direct 8 neighbors into account. A window size of 29 pixels[5] is larger than the width of the smallest fields in the test site.

3.3. Conventional Approach

The conventional approach involves two steps: First the endmember were determined with a method based on PPI and second these endmembers were unmixed with LSU approach.

The PPI was calculated according to Boardman et al. (1995). In this method, a pixel is defined as pure when it is at the end of a unit vector. At the end of the vector a threshold factor of 3 PCA band unity was used, in the sense that each pixel value within this range was counted as pure. There were 10,000 iterations. The PPI algorithm could not find a pure pixel for each crop type, when it was calculated on the whole scene. Instead, the pure pixels for each crop type were determined in a subset containing only the training data of the corresponding crop type. For the endmember selection of each crop type the mean value of the corresponding pure pixel values was calculated.

The LSU was done by SVD of the PPI derived endmembers (Boardman, 1989). It was calculated once with a unit to sum constraint of 1 (ASC holds true) and once without any constraints. An abundance map for each endmember and a root-mean-square (RMS) error image for unexplainable parts of the data set were calculated. Since

[5] 29 pixels correspond to 58 m, since the spatial resolution of the IS data is 2 m.

the calculations are done on the PCA reduced data set with only 7 bands, there is no unique solution for the ten crop type endmembers (Bioucas-Dias et al., 2013; Keshava and Mustard, 2002). This circumstance must be taken into account in the analysis of the results.

To have the possibility to compare the two methods, the LSU results were classified in a similar manner as the advanced classification of the proposed method.

4. Results

There are two main results for the proposed method and the conventional approach. On the one hand there are abundance maps of each crop type and on the other hand classification maps are generated. Since the classification is based on the abundances, the latter is shown first. However, both depend on the threshold values (Figure 3.11). It is conspicuous that there are a lot of overlapping ranges, but there are some differences as well, like *meadow young* and *rapeseed* in PCA band 3. There are some groups which have always overlapping threshold values or at least close together. One of these groups, further called SOIL, contains *bare soil*, *bare soil bright* and *sugar pea*. These types are separated in PCA band 2 from all the other crop types. The overlapping part of the threshold values of *bare soil* and *bare soil bright* becomes larger with higher PCA band number. In the first 2 bands they touch each other with a small overlapping part. They become larger in band 3 and 4. In the last 3 bands, the overlapping part is much bigger than the other.

Another group of crop types that belong together are the three crop types *spring barley*, *winter barley* and *winter wheat* and therefore called CROP. In PCA band 2 and 5 the range of the winter crops is totally captured by the range of *spring barley*. Additionally, the threshold values of *winter barley* are captured by those of spring barley in PCA band 1. Only in band 3 there is no overlapping between these two crop types. The values for *winter barley* and *winter wheat* overlap in every band. In band 3 is the smallest intersection, in band 7 *winter wheat* is captured by *winter barley* and in band 5 they are almost comparable.

There is a last group of similar threshold values, called MEADOW, with *alfalfa, meadow* and *meadow young*. Here the threshold values of *alfalfa* are always part of those of *meadow*. Since all pixels with values in the threshold range of *alfalfa* are in the *meadow* range as well, in each case results an abundance of (at maximum) 50% for *alfalfa*. *Meadow young* is part of this group, because the differentiation from *meadow* is done based on visual impressions. Only in the first and the last two PCA bands there are overlaps from the threshold values of *meadow young* with those of *meadow*.

The threshold values of *rapeseed* have also overlaps with those of other crop types, but not always with the same crop type. In band 3 it is clearly delineated. Hence it forms its own group called RAPESEED.

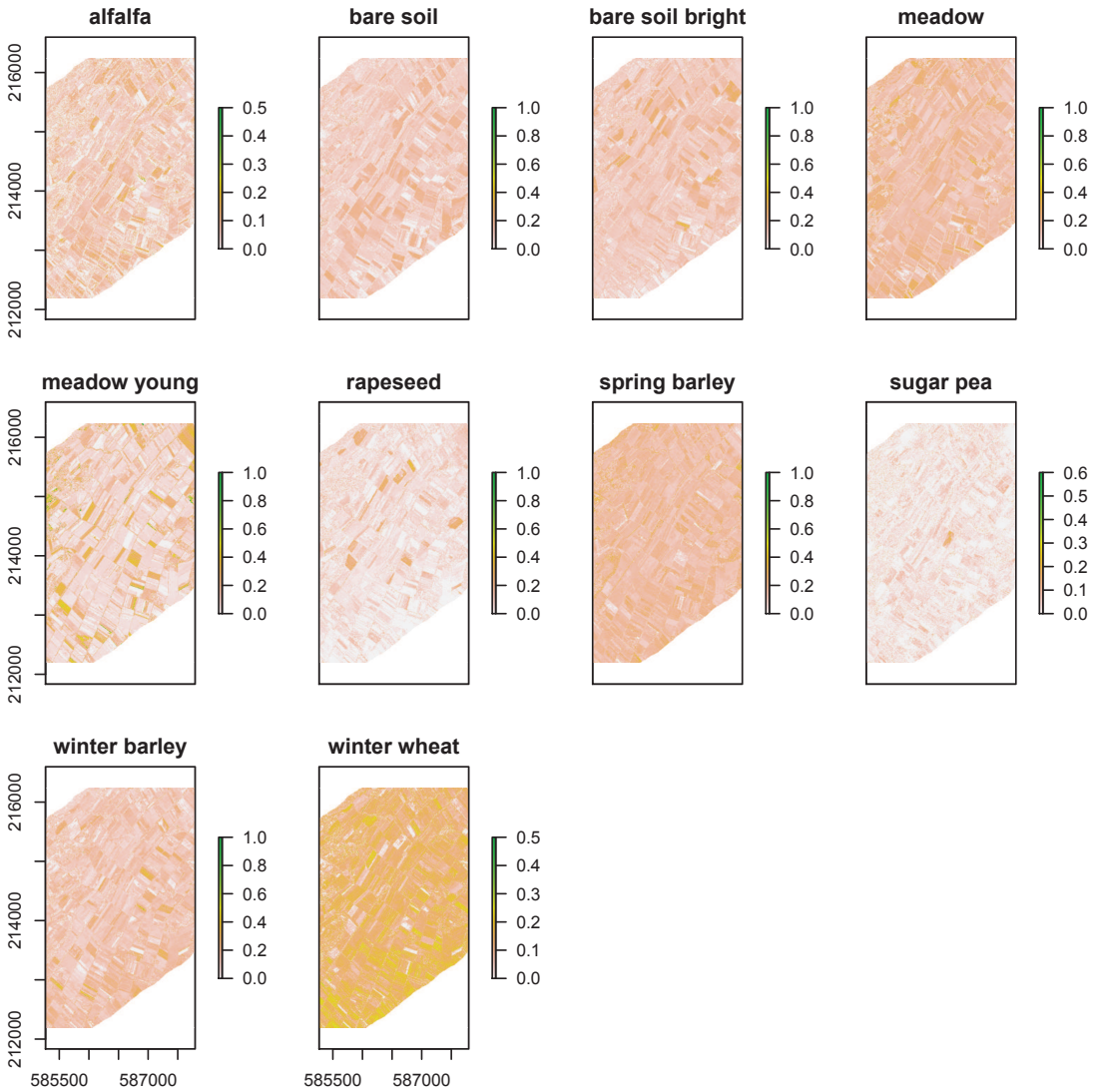

Figure 4.1.: Abundance maps of all crop types calculated by the proposed method. High abundances are plotted in green, low abundances in white and beige.

4.1. Proposed Method

4.1.1. Abundance

An abundance map is calculated for each crop type (Figure 4.1). The map shows high abundances of a crop type in green and low in beige. Pixels with abundance of zero or in case of no data being available (outside the flight strip in the north western and south eastern edges) are white. Overall there are only few pixels with high abundances. In all the maps the field structure of the scene can be seen. Some of the plots show obvious differences like *meadow young*, *rapeseed*, and *sugar pea*. For the *rapeseed* and *sugar pea* fields the higher abundances correspond well with the ground truth data. For the *meadow young* fields this effect is not visible. There are some crops with higher abundances, but they are not necessary of this type in the ground truth. There are also some high *rapeseed* abundances in *meadow young* fields.

Figure 4.2 shows the mean abundance in all ROIs of a certain crop type. For all cases except *bare soil*, *meadow*, and *spring barley*, the crop type with the highest mean value is the same as the corresponding ROI. In the other cases it is the second highest abundance. In *spring barley* fields, the abundance values of the three crop types *winter barley* (17.68% abundance), *spring barley* (17.30%), and *winter wheat* (17.28%) lay close together.

The abundance map for *sugar pea* shows the only *sugar pea* field in the test site with distinguishable higher values than other regions (Figure 4.1). In the northwest, the field adjoins *bare soil bright* and in the southeast *bare soil* (Figure 4.3a). However, there are two other crop types with higher values (Figure 4.3b) and some white patches with even highest abundances. Often there are exactly the same abundances for *meadow* and *bare soil* in these pixels. As it can be seen in the box plots of the abundances of the ten different crop types in the *sugar pea* field (Figure 4.4), *winter wheat* has as well rather high abundances. However, there are no pixels where *winter wheat* has the highest value. The higher values lay especially in the southern part of the field, where larger white areas can be found with similar abundances.

In the RGB image (Figure 4.3c), areas can be identified with unclear main membership in shades of brown, if all three crop types have similar abundances, or in shades of cyan, if *meadow* and *bare soil* have similar abundances and *sugar pea* a lower abundance. However, there is more area with *sugar pea* than expected in the classification with highest abundances. Most of the area with *bare soil* is colored in purple tones, therefore *sugar pea* is present there as well. Obvious are the lower abundances of *sugar pea* in the adjacent fields (Figure B.1).

All pixels have abundances greater than zero for *bare soil*, *meadow* and *spring barley* (Figure 4.4) and all these abundances are smaller than 30%. Most of the pixels have an abundance around 20% for *bare soil*, 15% for *meadow* and *winter wheat*, and 11% for *bare soil bright*, *spring barley* and *sugar pea*. The *sugar pea* type has the greatest variance and no outliers. *Meadow young* and *rapeseed* are the only two crop types with an abundance of 0% for most of the pixels.

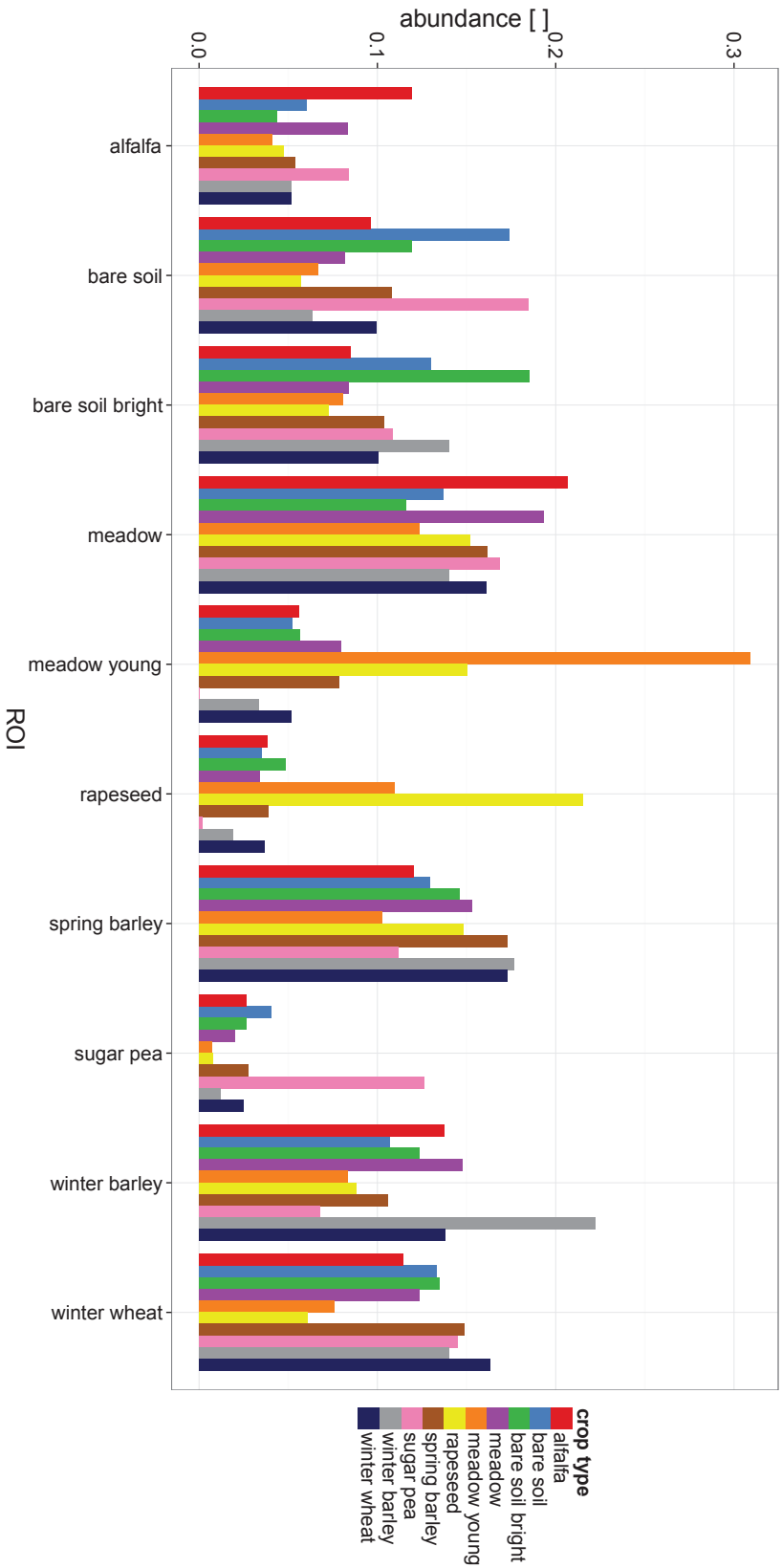

Figure 4.2.: Mean abundance of each crop type in all ROIs of a certain crop type.

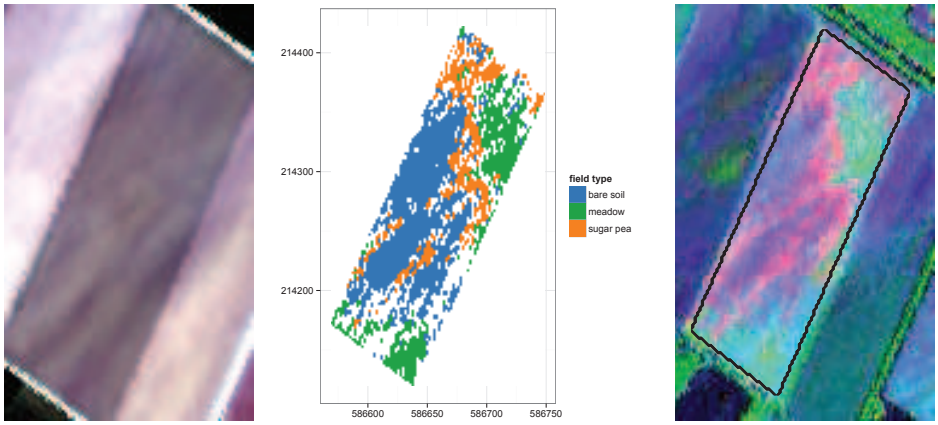

(a) (b) (c)

Figure 4.3.: Images of the *sugar pea* field as true color (a), classification with highest abundances (b) and RGB image with abundances of *sugar pea* (red), *meadow* (green) and *bare soil* (blue) (c). The black polygon is the contour of the *sugar pea* field ROI.

4.1.2. Classification

There are several classification results with different modal filter window sizes from 1 to 29 and methods (simple or advanced). In the classification image for a window size of 1, there are many patches with NA values as can be seen in Figure 4.5 showing the advanced classification. As mentioned above, these NA patches occur when multiple crop types have the same value of highest abundance. These patches are classified randomly in the simple method with one of the classes with highest value. NA values in the advanced classification method are treated as unclassified. The OA is 39.66% for the advanced classification method and 47.90% for the simple method for a window size of 1. That corresponds to no filtering and therefore to the maximum pixel value of the mixture analysis. Detailed confidence matrices can be found in the Appendix B.2.

For both methods the OA increases for larger extents of the modal filter (Figure 4.6a and Table B.1 and B.2). The OA reaches a stable value around 54% already for small window sizes and 53.49% for a window size of 7 with the advanced method, which is less than 2% under the maximum value of 54.45%, reached by a window size of 19 (Figure 4.6a). For a window size of 11 the OA is 54.07% which corresponds to less than 1% under the maximum. For the simple method results are slightly different (Figure 4.6a). The slope is less extreme than with the advanced method and reaches the maximum of 54.24% with a window size of 23. An OA of 53.28% by a filter size of 13 is less than 2% under the maximum and 53.40% by a filter size of 15 is less than 1%. The kappa coefficients, calculated with a method after Cohen (1960) and Hudson and Ramm (1987), are between 0.06 and 0.085 and therefore almost 0. In both cases the classification map for maximum OA is very smooth and shows only few patches of other crop types in a field (Figure 4.7).

The user accuracy (UA) and producer accuracy (PA) show for both methods similar behaviors (Figure 4.6b and 4.6c). They increase rapidly within the window sizes of 1 to

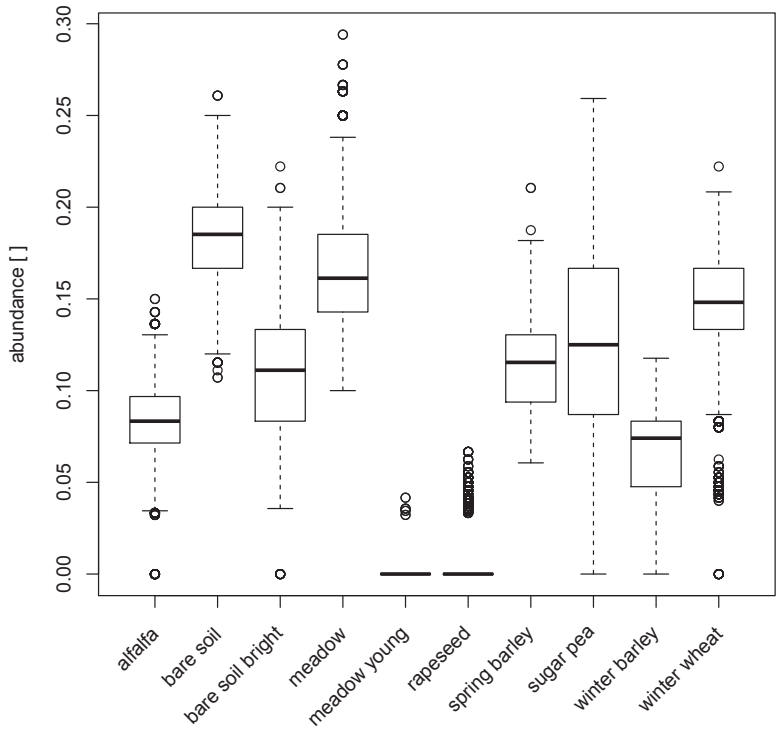

Figure 4.4.: Box plots of the abundances in the *sugar pea* field.

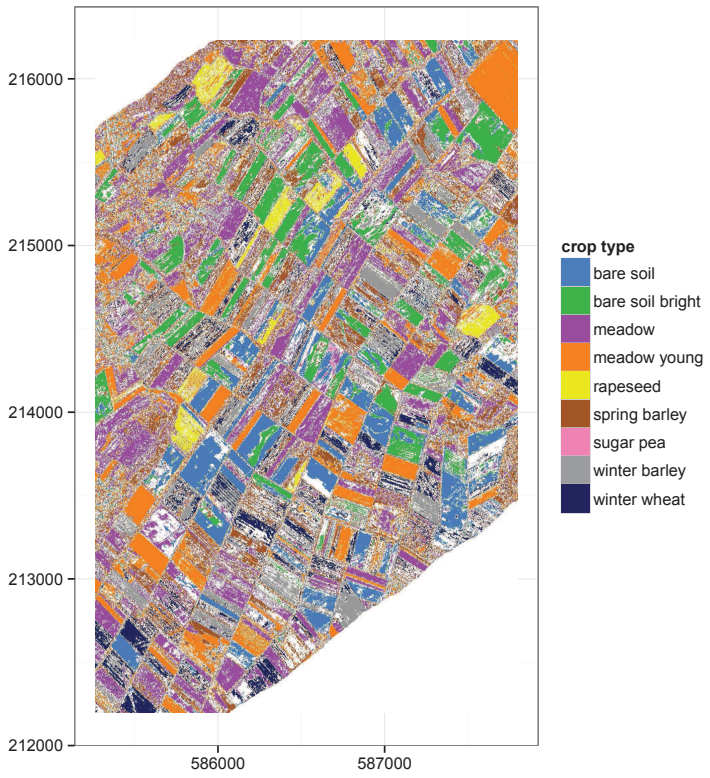

Figure 4.5.: Advanced classification with modal filter window size 1 of the proposed method.

5 and then rise only slightly to the maximum around the window size of the maximum OA. Afterward there is a small decrease. The producer accuracies of *spring barley*, *sugar pea* and *winter wheat* have their maximum in the first window sizes. The UA shows a decrease from window size 1 to 3 in case of the advanced method, but otherwise a similar behavior as the UA. The UA for *sugar pea* has a strange curve progression. It falls from 100% at a window size of 11 to 0% at a window size of 13. The PA falls from a level below 10% at window size 3 down to 0% at window size 13. In case of crop type *alfalfa* the PAs of both methods are 0% and the UAs 0% or NA. NA values result because no pixels are classified as the corresponding crop type and thereby a division by zero occurs. Therefore NA could be also interpreted as 100%. In the group of unclassified pixels in the advanced classification, the PA is always NA, because there are no pixels unclassified in the control data. Therefore the PA is always 0%.

There are only small differences between the two methods for the UA and PA. Obvious is the difference between UA and PA itself. *Rapeseed* shows for both methods an UA around 100% and a PA between about 60% and 80%. *Meadow young* has a PA around 100%, but the UA is around 60%. *Spring barley* and *winter barley* have both an UA around 20%. The PA is higher with a maximum of around 45% for summer and 75% for winter type. *Winter wheat* shows an inverted behavior with a PA around 20% and an UA around 70%. For the other crop types the differences between UA and PA are

smaller, but show the same inverted behavior between the two accuracies.

There are crop types that are difficult to discriminate from each other. The types' *bare soil* and *bare soil bright* have an obvious difference, but there is no clear boundary value between these two classes. The same is true for *meadow* and *meadow young* field types. On the other hand there are different crop fields with barley and wheat and in case of barley spring and winter species. They count all to the same order (poales), family (poaceae), subfamily (pooideae), and tribe (triticeae) and differ only in the genus (triticum or hordeum, respectively).

These difficult distinguishable crop types are merged to the already mentioned groups' CROP, MEADOW, RAPESEED and SOIL, but the two crop types with few training data (*alfalfa* and *sugar pea*) are left out. With these restrictions the OA increases (Figure B.2). As with all ten crop types, the simple method shows with small window sizes (1 and 3) a higher OA than the advanced method. The highest OA which can be reached is 79.12% for a window size of 19 for the advanced method and 78.68% for a window size of 23 for the simple method. The best kappa coefficients are reached at the same window sizes and are 0.283 for the advanced method and 0.281 for the simple method. Both values are slightly better for the advanced method.

4.2. Conventional Approach

4.2.1. Abundance

For the PPI derived endmembers a certain number of pure pixels depending on crop type have been investigated (Table 4.1). The mean values in the first two PCA bands are different (Figure 4.8). With higher band numbers they become more similar, except *rapeseed* which has different values in PCA band 3 and 4. Overall, they show a similar grouping effect with the same four groups like the threshold values of the proposed method.

Table 4.1.: Number of pure pixels for each PPI endmember.

crop type	number of pure pixel
alfalfa	170
bare soil	177
bare soil bright	171
meadow	247
meadow young	216
rapeseed	194
spring barley	230
sugar pea	207
winter barley	225
winter wheat	239

The LSU is calculated with two different methods: once with a sum to one constraint (or ASC of 1) and once without any constraints. The constrained version shows abundance maps with a field pattern as can be expected based on the test site (Figure

4.9). High values are plotted in green, low values in white and beige. The abundances are stretched for each map individually and therefore green values correspond to abundances around 200 in case of *spring barley* and abundances around 40 in case of *alfalfa*. There are very high values around 200 and very low values around -150. However, high abundance values correspond not always with the crop type. An example is the endmember for *rapeseed* which has lower abundance fractions in *rapeseed* fields than in the fields with highest abundance fractions. Conspicuous are the stripes in the southeast with higher values for *spring barley* or *rapeseed* and lower values for *winter barley* or *meadow young*.

The abundance maps of the unconstrained version show less distinct fields and are more noisy, except for *rapeseed* (Figure 4.10). The values are much smaller for the unconstrained version than for the constrained version. Only the abundance map of *rapeseed* shows higher abundances in the corresponding fields.

The error image shows higher abundances for both versions for field borders, streets, water and in urban regions. The fields are either homogenous or noisy.

4.2.2. Classification

The classification is done according to the proposed method with the advanced classification method. Both methods show less noisy classification maps (Figure 4.11). For the constrained version there are no unclassified pixels, for the unconstrained version there are only 41 or 0.0138% unclassified pixels in *winter wheat* fields. The detailed confidence matrices for the highest OA can be found in Table B.7 and B.8 in the Appendix.

In the classification of the constrained LSU most pixels are classified as *sugar pea*, followed by *spring barley* and *winter barley*. Conspicuous is the *spring barley* stripe in the southeast. The crop type *meadow* is the only type showing a distinct pattern, unfortunately 79.4% of the pixels are *rapeseed*, whereas the most distinct classified *rapeseed* field in the southeast is *meadow*. The OA is 5.93%, the kappa coefficient is 0.00827. Both decrease with modal filtering. *Winter wheat* has a PA of 15.6% and a UA of 60.9%, *meadow young* has a PA of 23.8% and a UA of 28.2%. For all other crop types the PA and UA are below 5%.

The classification of the unconstrained LSU shows more distinct fields and the same stripe effect in the southeast. Again, most pixels are classified as *sugar pea*, followed by *spring barley*. Third are pixels classified as *winter barley*. In contrast to the classification of the constrained LSU, in the unconstrained version *rapeseed* is classified correctly. The PA is 80.2% and the UA 98.5%. *Sugar pea* has a PA of 90.3%, but a UA of only 1.34%. For *winter wheat* the contrary effect is true and the PA is only 8.57% whereas the UA is 90.4%. All the other accuracies are below 75%, partly even in the single digit range. Therefore the OA is only 22.9% and the kappa coefficient 0.0355 for a modal filter window size of 1. These values slightly increase for a modal window size of 5 to an OA of 23.4% and a kappa coefficient of 0.0363. For larger window sizes these values decrease.

4.3. Comparison of Abundances

To compare the abundances of the proposed method and the conventional approach, the R^2 values between the proposed method and each of the two conventional approaches are calculated (Table 4.2). The highest congruity can be found for the constrained ($R^2 = 0.167$) and unconstrained ($R^2 = 0.186$) version for *rapeseed*. The R^2 values are greater than 0.12 for *meadow young* in case of the constrained and *winter barley* in the unconstrained version. For all others crop types the values are below 0.1, for *spring barley* and *alfalfa* in the constrained version very low (smaller than 0.0001). The mean R^2 value for the constrained version is 0.0447 and 0.0458 for the unconstrained version.

Table 4.2.: R^2 between the proposed method and the two conventional approaches.

crop type	constrained	unconstrained
alfalfa	0.00003	0.03000
bare soil	0.00031	0.02359
bare soil bright	0.04127	0.02423
meadow	0.02742	0.00068
meadow young	0.12647	0.04952
rapeseed	0.16665	0.18558
spring barley	0.00006	0.00587
sugar pea	0.03325	0.00129
winter barley	0.03845	0.13339
winter wheat	0.01303	0.00344
mean	0.04469	0.04576

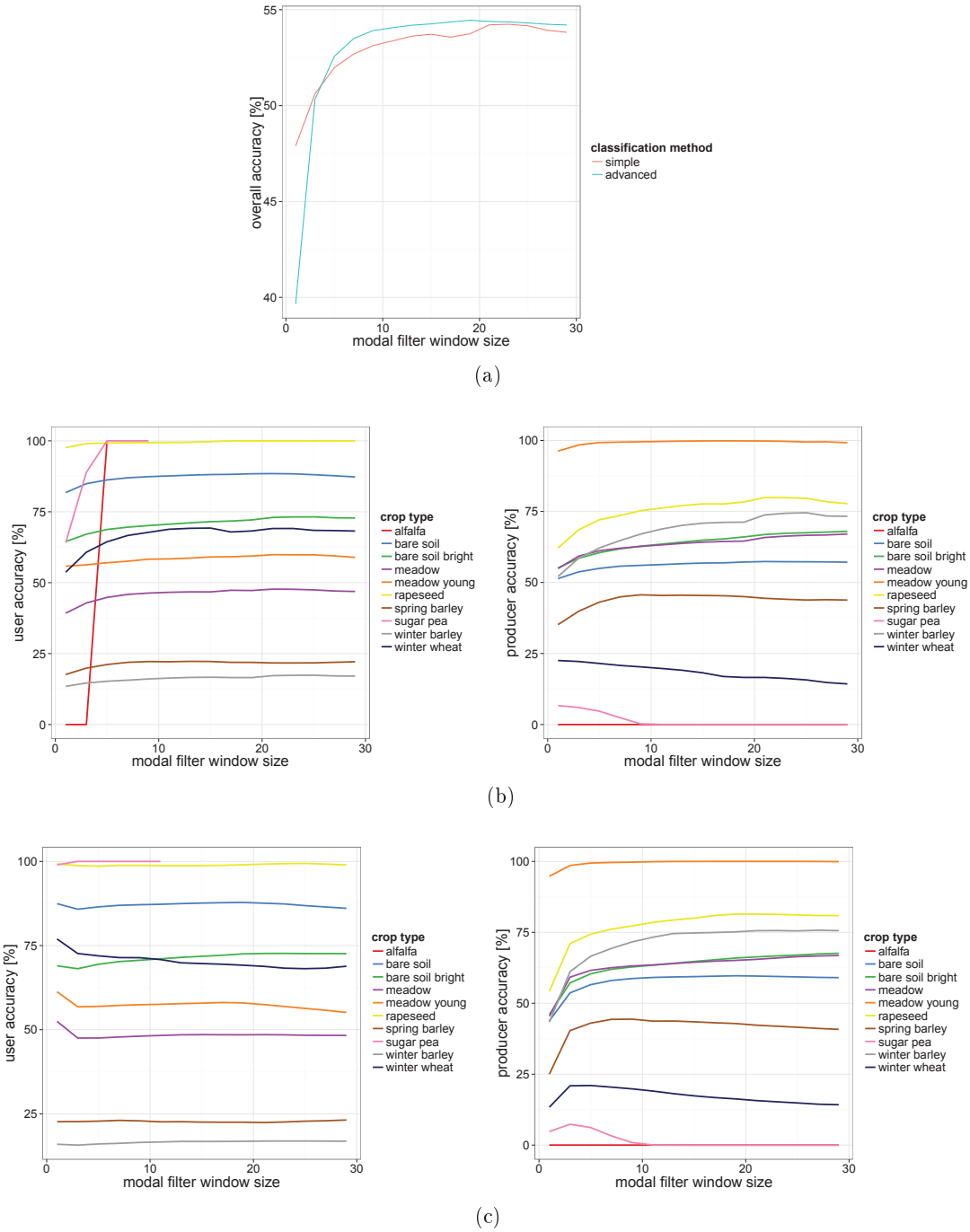

Figure 4.6.: Changes in overall accuracy for simple and advanced method (a), user and producer accuracy for simple (b) and advanced method (c).

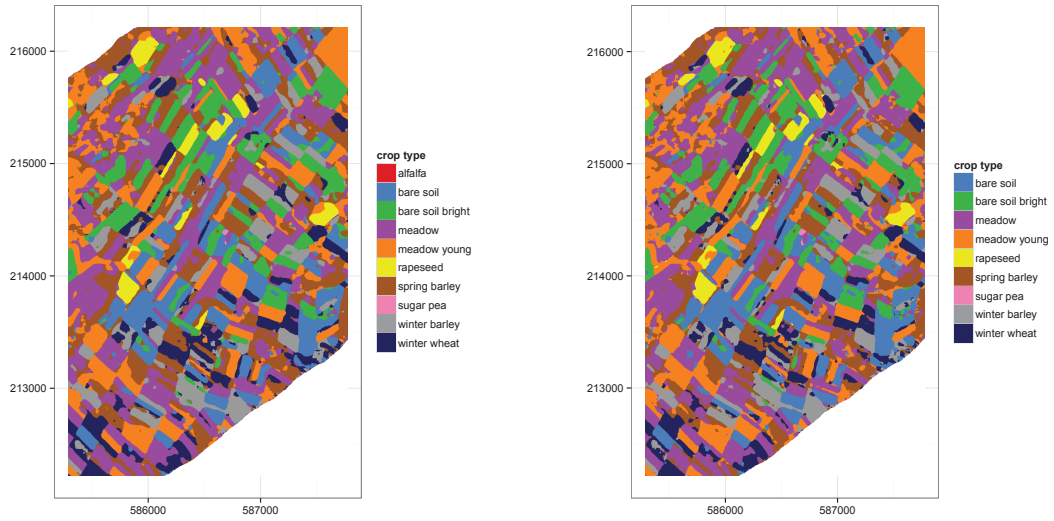

Figure 4.7.: Classification maps for maximal overall accuracy for simple method (a) and advanced method (b).

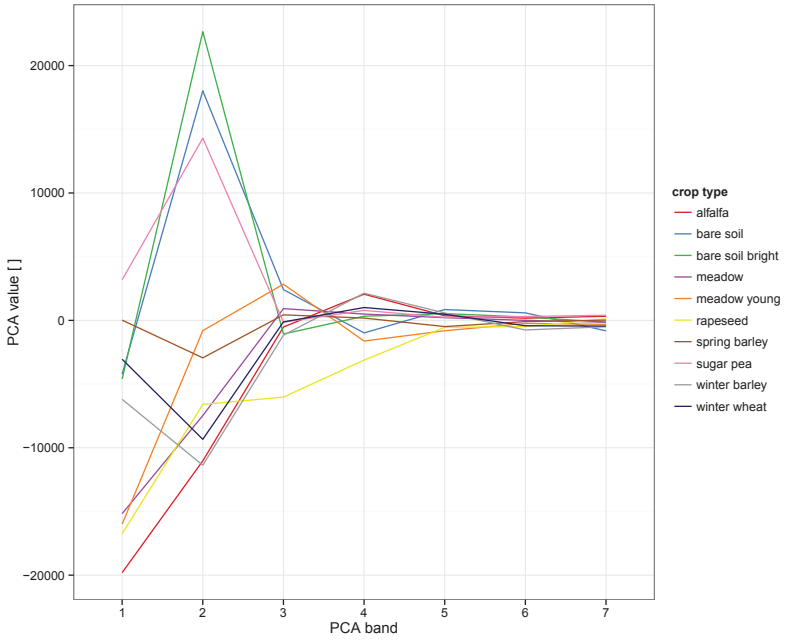

Figure 4.8.: Mean of PPI derived endmember values.

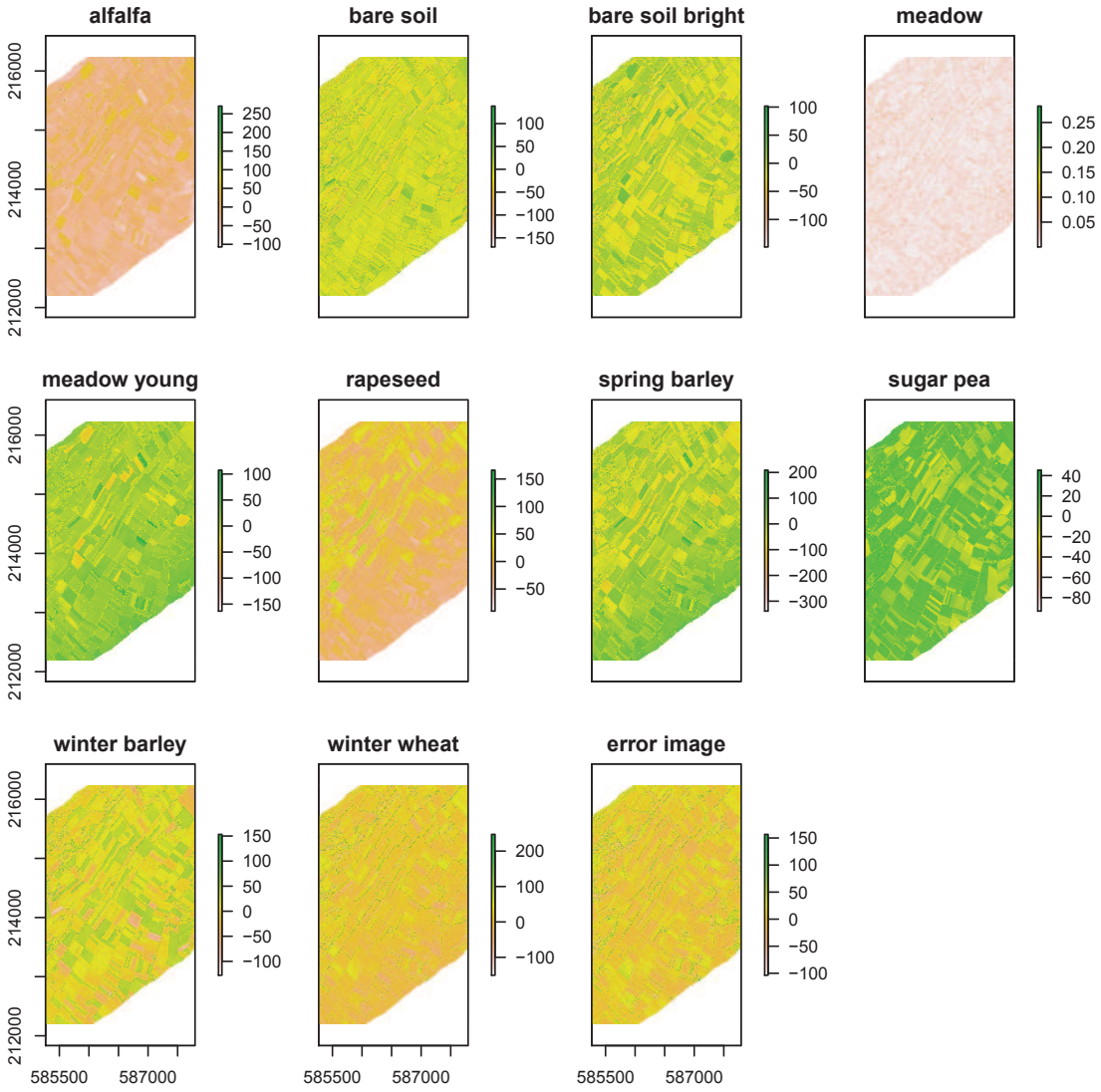

Figure 4.9.: Abundance maps and error image of LSU with PPI derived endmembers and a sum constraint of 1. Green are high abundances, white and brown low abundances.

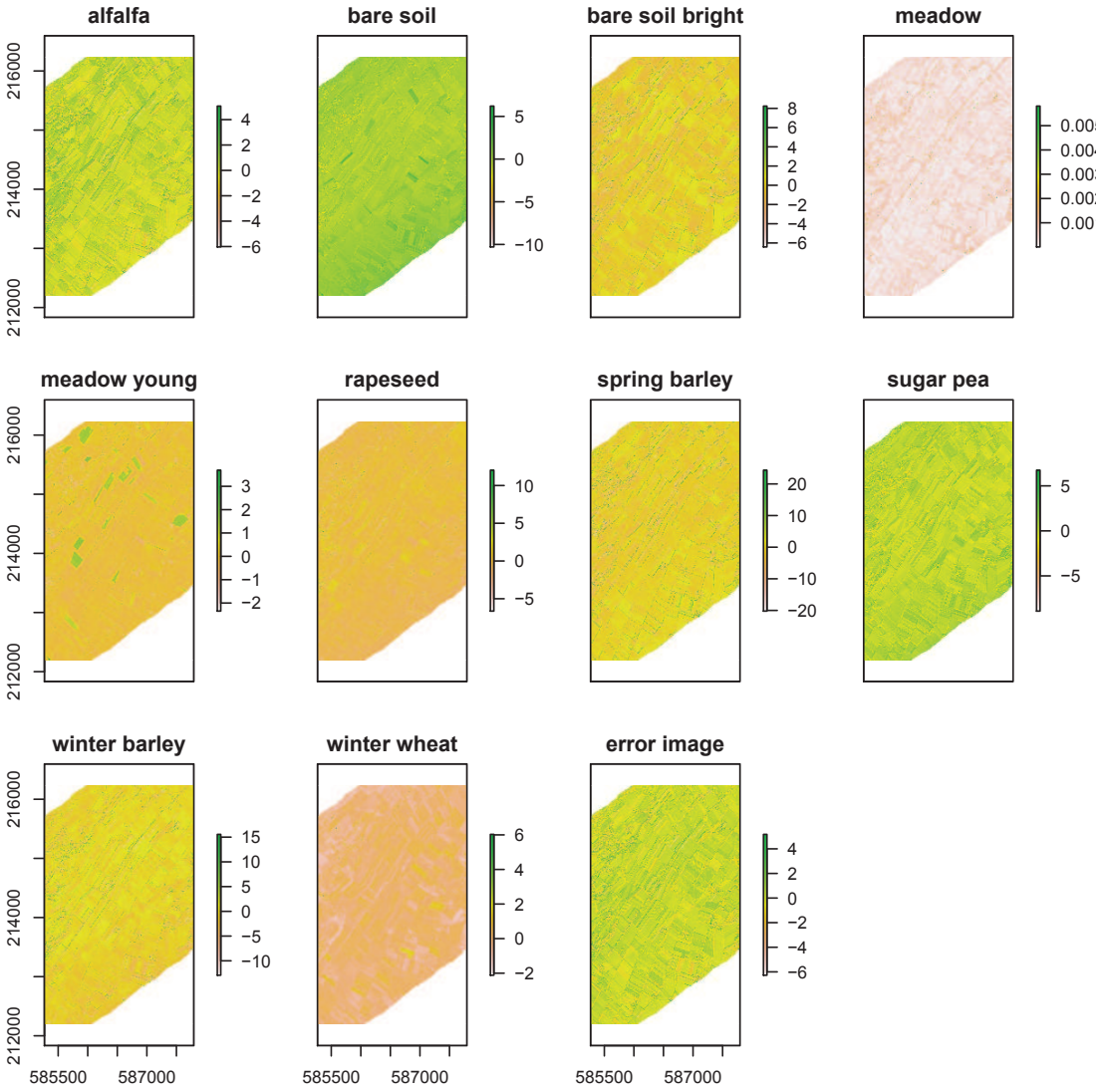

Figure 4.10.: Abundance maps and error image of LSU with PPI derived endmembers. There is no sum constraint. Green are high abundances, white and brown low abundances.

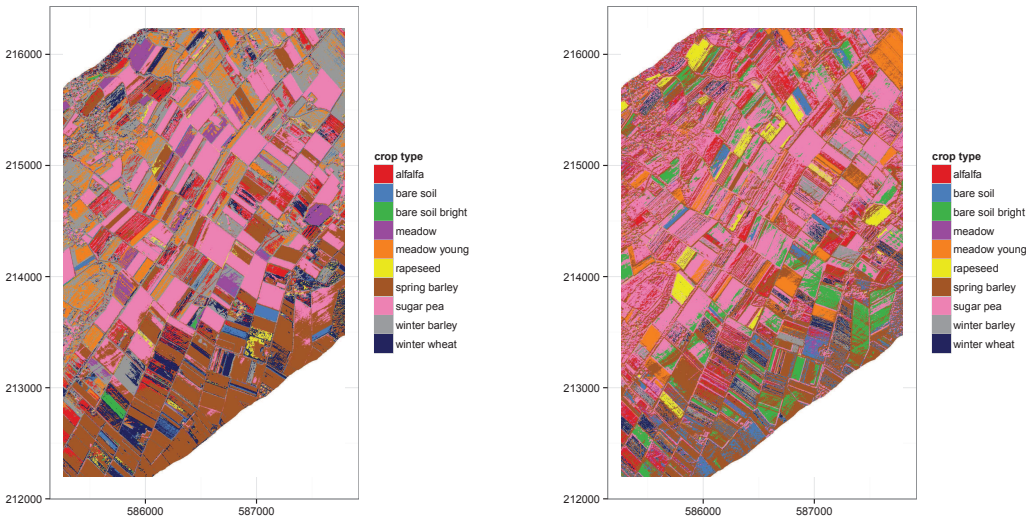

(a) (b)

Figure 4.11.: Classification maps with highest abundance values of constrained (a) and unconstrained LSU (b) (modal filter window size 1). Classified with the advanced method.

5. Discussion

This chapter is divided into four parts. In a first section the spectral behavior of agricultural crops recorded in May is discussed. Further the data reduction method is discussed since both applied methods use the reduced data. The following two parts address the proposed method and the conventional approach. The last section focuses on a comparison of the proposed method with the conventional approach.

5.1. Spectral Behavior

5.1.1. Crop Plants in an Early Stage

The distinction of different crop types in the present IS data is difficult due to the early stage of plant development. As mentioned above, some crop types are spectrally rather similar (Figure 2.6) and therefore affect the threshold values in the proposed method and the PPI derived endmembers in the conventional approach. A study about *winter wheat* in early plant development (stage 1 and 2 in BBCH scale in the November) shows very low vegetation coverage rates (Torres-Sánchez et al., 2014). Therefore a lot of *bare soil* information is contained in a pixel of plants that are sown in narrow crop rows (Torres-Sánchez et al., 2014; Hengl, 2006). Due to missing ground truth at the image recording time the exact stage of the plants can only be estimated. Consequently, the vegetation coverage and soil fraction in the fields is unclear. *Rapeseed* is present in two stages (flowering and before flowering). Therefore, the non-flowering parts of *rapeseed* fields have higher abundances for *meadow* than for *rapeseed* and are classified accordingly.

Foerster et al. (2012) uses normalized difference vegetation index (NDVI) values of four phenological useful IS data sets for his study of agricultural crops. They found plant groups for winter crops, summer crops and perennial field grass and fallow (Foerster et al., 2012). The groups are slightly different from the groups found in this work, which can be explained by the analysis of multiple stages by Foerster et al. (2012). *Rapeseed* is part of the winter crops, and these can be distinguished from the summer crops. The NDVI of grass becomes larger with increasing growth state and is clearly different from fallow. Cut grass fields have a similar NDVI as fallow and they are therefore grouped together. A differentiation of these crop types based on the NDVI of a single acquisition in May seems difficult.

5.1.2. Data Reduction

The reduced data set with only seven bands proved to be sufficient for successful application of the proposed method, but it does not contain enough spectral information for the conventional approach based on PPI and LSU. For a conventional LSU of 10 endmembers at least 10 bands would be required (Bioucas-Dias and Plaza, 2010). Hence,

the stripe effect in the PCA bands reinforces with further bands, a proper LSU is not possible on the reduced data set. Nevertheless, the conventional approach was followed with the same data set, because of comparability reasons.

In the proposed method threshold values are calculated to distinguish between the crop types. This threshold values sometimes have large overlaps and some are totally captured by others. Therefore clear differences between the threshold values would be preferred. A calculation of the PCA transformation statistics based on a spatial subset to agricultural fields and a following application to the whole data set would possibly lead to a better result that shows more distinguishable values for crop types. Under the aspect of computational load and data volume a data reduction is mandatory for the proposed method and at least desirable for the conventional approach.

5.2. Proposed Method

The original idea was to use the variogram cloud for the endmember determination. As mentioned already in the methods, the variogram is a measure of spectral dissimilarity (Jupp et al., 1988) and therefore the most similar pixels can be extracted from the variogram cloud. In case of *alfalfa* the computational load is acceptable. The most spectrally similar pixels are neither distributed over the whole field nor clustered (Figure 5.1). Since the computational load increases as a quadratic function of the number of pixels, an application to other crop types requires weeks and memory of more than 6 GB. The quadratic increase is based on the fact that each pixel value is compared to each other pixel value and therefore the number of comparisons equals $1/2 * n * (n-1)$, where n is the number of pixels.

The ambition to incorporate spatial information in the unmixing model can only partially be filled by the variogram. The variogram is defined for 2 or 3 dimensions (Chilès and Delfiner, 2012). Therefore the variogram in remote sensing is used for 2 spatial and one z-dimension in combination with kriging (Atkinson and Lewis, 2000) or Monte Carlo methods (Bioucas-Dias et al., 2013). This surface phenomenon could be represented by the NDVI (Garrigues et al., 2008a), the leaf area index (Garrigues et al., 2008b) or other indexes.

In the proposed method the variogram is used for threshold estimation to provide a probability density function. There are alternative statistical parameters for a threshold value that are computationally less complex like the standard deviation or quantile. Perhaps the upper and lower quartile is an alternative to the variogram approach (Appendix B.3), since the difference between quartiles (end of box) and the threshold value (red points) based on the variogram is small. Further, Atkinson and Lewis (2000) propose to use variance and covariance between wavebands for an improved probability distribution.

Due to the overlapping threshold values most of the pixels have abundances greater than 0% for almost all crop types. In case of the *sugar pea* field all abundances are smaller than 30%, as mentioned in the results. Therefore the calculated abundances do not represent the real fractions of the pixel but can be interpreted as membership of a crop type in a pixel (Schowengerdt, 1996; Villa et al., 2011). The membership comes closer to the truth than a hard classification, as can be seen also at the *sugar pea* field. In the classification only few pixels are classified as *sugar pea* (Figure 4.3b), but there is

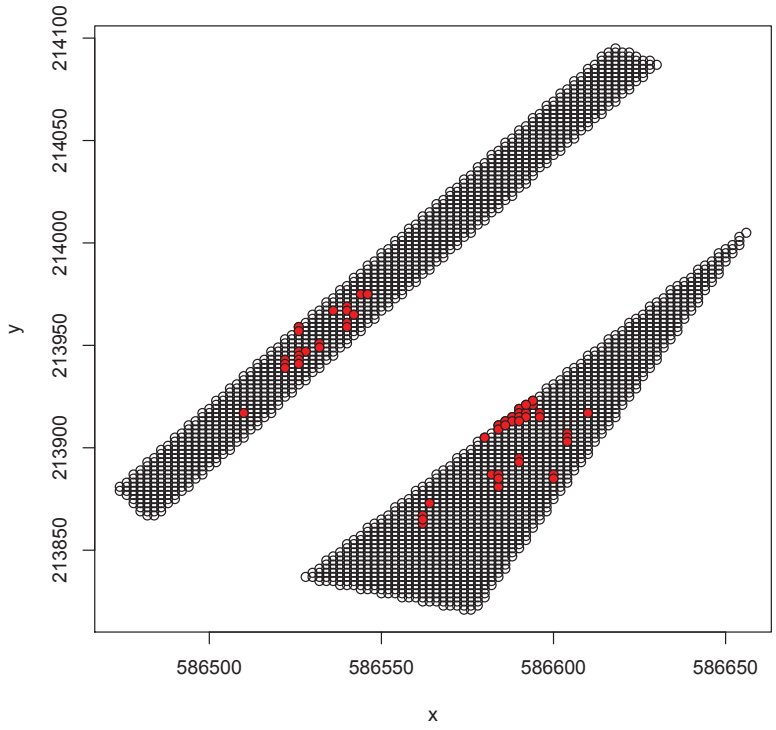

Figure 5.1.: Most spectrally similar pixels in the *alfalfa* training fields calculated with the variogram cloud based approach.

much more of *sugar pea* as expected due to the classification as the RGB-image shows (Figure 4.3c).

5.3. Conventional Approach

A proper linear unmixing is possible only, if the number of endmembers is at most as large as the number of data bands (spectral, PCA, etc.) plus one. Otherwise the endmembers are not linearly independent and unmixing leads to results that are not unique (Keshava and Mustard, 2002; Bioucas-Dias et al., 2013). In this work a data set with seven PCA bands was used for the unmixing of ten endmembers and consequently the endmembers must be linear dependent. The endmembers show the same grouping effects in the mean spectra of the crop type ROIs, the endmember spectra and the threshold values of the proposed method.

Therefore the results of the conventional approach are not unique and show arbitrarily high abundances. Especially the abundances are too large for the constraint version. Abundances greater than 1 or less than 0 do not have a physical meaning and indicate usually a bad model fit and endmember determination (Plaza et al., 2004). Normally, values less than 0 are set to 0 and such over 1 to 1, but in the present case this seems to be unreliable as it violates the ASC.

Maybe this is a problem of the pureness of the image derived endmember. It is possible that for some crop types even the purest pixels have a larger fraction of soil in it. It is possible that early vegetation growth took place in *bare soil* and *bare soil bright* fields already. As the ground truth took place months later, this question cannot be answered conclusively.

5.4. Validation of chosen methods

Validation of SMA results is a general problem when ground truth is not available (Keshava and Mustard, 2002). A detailed knowledge of the content of a pixel is necessary for a proper validation. In the validation of unmixing results of satellite data it is a widely applied approach to use finer resolution satellite data (Xie et al., 2008). For the validation of an algorithm synthetic data can be used, because the mixture of each pixel or the distribution of a certain phenomenon is exactly known, as Woodcock et al. (1988) applies. In the unmixing of crop residues Bannari et al. (2006) use photographs of different directions, Peddle and Smith (2005) use video data in their study and Torres-Sánchez et al. (2014) acquire data with an unmanned aerial vehicle (UAV) in the visible region of the spectrum with ultra-high spatial resolution (1-2 cm). It must be taken into account that this high-resolution data must be interpreted as well, which can potentially lead to errors (Defries and Townshend, 1999). Since no additional information is available for the test site, the proposed method was compared to a conventional approach and validated with a classification of the unmixing results.

5.4.1. Unmixing Results

The ANC and ASC are fulfilled for the proposed method. In case of the conventional approach the ASC is only fulfilled for the constrained version of the LSU. This leads to

very different data ranges for the resulting abundances. The fields in the present test site can be seen as checkerboard and abundances correspond to the part of surface in a pixel covered by the corresponding endmember. Therefore only abundances between 0 and 1 are reliable. As mentioned above, this requirement cannot be fulfilled for the conventional approach. Since the abundances of the proposed method and the conventional approach have different data ranges the R^2 values are calculated, under the assumption that there is a linear relationship between the two scales. The reason is that this measure is tolerant towards different scales. In particular the smallest abundance value in the proposed method is 0 and in the conventional approach it is always negative. Therefore, both have the meaning of total absence of the crop type. The same assumption is made for the highest values.

There is only a weak relationship between the abundances of the proposed method and the conventional approach, since all R^2 values are below 0.2. First of all, this could be an effect of the linear dependence between derived endmembers and the therefore faulty results of the conventional approach. It is obvious that the highest R^2 values appear for *rapeseed*. The field structure for this crop type is easily recognizable in all three abundance maps already. The same is true for *meadow young* with the second highest R^2 value in the constrained conventional approach. For the unconstrained conventional approach the field structure is not easily recognizable anyway.

Another reason for low R^2 is the absence of an error part in the proposed method in contrast to the conventional approach. The ambition of the LSU in the conventional approach is to explain the values of a pixel as much as possible by linear combinations of the PPI derived endmember spectral library. Since this is not always possible, an error term is left. For example there are no endmembers for man-made structures in the spectral library, like buildings or streets. This leads to higher values in the error image for pixels that cover streets and consequently to low or in the best case to no abundance for a crop endmember. For the proposed method the unmixing of such pixels is a problem. Since there are only threshold values for crop types included, the mixture of a pixel that covers a street is explained by crop types. Due to the fact that the ASC always holds true, the abundances of crop types of a certain pixel can get high. In the present test site there are almost always meadow stripes between the farm tracks and the actual used field. Consequently these pixels have high abundances for *meadow* as can be seen in Figure 4.3c[1]. Since there are comparatively few man-made structures this explains only a small part of the low R^2 values. The larger portion is caused by the poor unmixing of the conventional approach as the accuracy of the classification shows. This is discussed in the following paragraph.

5.4.2. Classification

The OA of the classification of the highest abundances for the conventional approaches are poor. In the best case the OA is 5.93% for the constrained and 23.4% for the unconstrained version. The kappa coefficient is near zero, i.e. there is a slight strength of agreement (Landis and Koch, 1977). The modal filter does not improve the classification of the constrained version and has a small influence on the OA of the unconstrained version (22.9% without filtering and 23.4% with a modal filter window of size 5). This

[1] Field tracks are visualized with very bright colors in the true color image (Figure 4.3a).

leads to the conclusion that highest abundances in a certain field are stable and do not change pixel by pixel.

In the proposed method the modal filter influences the OA and leads to an increase of 6.34% for the simple classification and 14.79% for the advanced classification. The best OA is 54.24% for the simple classification by a modal filter window of size 23. It is slightly better for the advanced classification by a modal filter window of size 19 with 54.45%. In other words, a bigger window size is required to rectify the misclassified pixels in the simple classification. If no filter is used the simple classification method is reliable, because it does not select from all crop types but only from the (usually two to three) crop types with the highest abundance. The PA and UA are very similar (±2.4%) for the best (highest OA) classifications. Although the OA is much better than for the conventional approaches, the kappa coefficient is still very low, which means that there is also only a slight strength of agreement.

The disadvantage of the median filter can be seen in the classification of *sugar pea*. With a filter of window size 11 applied, the crop type of the neighboring field gets a higher influence on a pixel in the *sugar pea* field, which leads to misclassification. This effect is supported by the few properly classified pixels (Figure 4.3b).

Since the best simple and advanced classifications are very similar, in the following the classification of the proposed method denotes the best modal filtered advanced classification (window of size 19).

There is no reference data for man-made objects, therefore they have no influence on the accuracy of the classification compared to R^2. The largest accordance or highest R^2 in the abundances can be found for *rapeseed*. This is also evident in the classification for the proposed method and the unconstrained conventional approach. Both have high values for UA and PA (Table 4.7b and Table B.8). In the constrained version the R^2 for *rapeseed* is the highest as well, but the UA and PA are 0%, because the majority of *rapeseed* pixels are classified as *meadow*. There are two other values that are remarkable. The PA for *sugar pea* is 100%, because 38.1% of all pixels are classified as *sugar pea*. The UA is therefore only 1.77%. The other high value is the UA for *winter wheat* (UA = 61%), but the PA is only 15.57%. This relativizes the higher values. The other PA and UA values are all fewer than 30%. In the unconstrained version there are also high values for UA and low values for PA or vice versa for *spring barley*, *sugar pea* and *winter wheat*. Only *meadow young* and *winter barley* have UA and PA values over 55%, beside *rapeseed*. For the proposed method there are three crop types (*bare soil*, *bare soil bright* and *meadow young*) beside *rapeseed* with UA and PA over 55%. It can be concluded that the constrained conventional approach has no PA and UA over 55% for the same crop type, whereas for the unconstrained version this is true for *meadow young*, *rapeseed* and *winter barley*. In the case of the proposed method both the UA and PA are over 55% for *bare soil*, *bare soil bright, meadow young* and *rapeseed*. The proposed method has UA and PA fewer than 50% at the same time only for *spring barley*, beside *alfalfa* and *sugar pea* for which no pixel has been classified. For the unconstrained version of the conventional approach there are at least some pixels correctly classified for all crop types. However, there are four crop types with both UA and PA fewer than 50%.

High UA and low PA or vice versa seem to be a problem in a classification of ten or more crop types, since Foerster et al. (2012) report similar results. They completely failed in the classification of *meadow*, *meadow young* and partially *spring barley* (they

proposed a single class for all summer grains). For *winter barley* and *winter wheat* they have a better UA and PA and for *bare soil* and *bare soil bright* they have s slightly better UA and PA than in the classification of the proposed method. For *rapeseed* they have the higher PA with 93.3%, but only a UA of 49.2%, whereas the proposed method has a PA of 81.41% and an UA of 99%. Overall the proposed method classifies *rapeseed* and *meadow young* better and Foerster et al. (2012) has better accuracies for *winter barley*, *winter wheat* and *bare soil* and *bare soil bright*. The better OA (65.7%) of Foerster et al. (2012) can be explained by the fact that they used four data sets at different times of the year.

6. Conclusions

Crop mixture by intercropping on the same field is an important measure in agriculture because it can reduce the use of fertilizers or increase the yield of a field (Li et al., 2013). Timely available information about crop plants is useful for a variety of applications. Remote sensing offers this opportunity and IS data allows furthermore to do analysis at subpixel level. Conventional approaches show severe difficulties to capture the variation in vegetation-dominated scenes.

This thesis aims to distinguish ten different crop types on a subpixel level. The IS data acquired in May 2013 show a rural landscape, typical for the Swiss midland. To capture the spectral variability of the crop types a new method was proposed. The spectral variability is thereby captured with a variogram based approach that calculates the similarity between pixels of the same crop type. Threshold values are derived from this similarity values and transformed to density functions that allow the subsequent unmixing based on Bayes' theorem. The following conclusions are drawn by answering the four subordinate research questions and re-thinking the main objective posed at the beginning.

1. *Are there spectral differences between crop plants in an early stage of development?*
   There are partially spectral differences between the different crop types and in the present scenario they can be grouped into SOIL, CROPS, MEADOW and RAPESEED. This is due to the early stage of plant development, and because plants are very similar, i.e. *meadow* and *meadow young*. The two meadow types and *bare soil* and *bare soil bright* are separated manually based on visual differences. *Alfalfa* is not distinguishable from *meadow* due to complete overlapping of the threshold values. The three crop types are of the same tribe and summer and winter types are very hard to discriminate in June as well.

2. *Can the chosen proposed method explain the mixture in a pixel?*
   Due to the partially large overlaps of the threshold values, the unmixing in the proposed method produces abundances for the most crop types in the majority of the pixels. Therefore, each crop type has at least very small abundances for the majority of all pixels, which cannot be true. Hence, it is only possible to make a statement about the membership and not about the fractional composition of a pixel. Due to missing data for validation and the fail of the conventional approach (see subordinate research question 4) this question cannot be answered conclusively.

3. *Is the proposed method more suitable for classification?*
   There is an OA of 54.45% for a modal filtered classification of the main membership at a pixel and a kappa of 0.08 that corresponds only to a slight strength of agreement. Therefore, the proposed method is not suitable for a classification of all ten crop types. There are better classification results for *rapeseed* (both the

PA and UA are over 80%) and for *bare soil*, *bare soil bright* and *meadow young* (both the PA and UA are over 55%).

4. *How does the proposed method perform compared to a conventional approach based on PPI and LSU?*
   It is not possible to quantify the mixture reliably with the conventional approach. This is caused mainly by the spectral similarity of the crop types, the fact that the PPI does not find pure pixels for all crop types, when it is executed on the whole IS data set, and that there are a lower number of bands in the reduced data set than number of crop types. This leads to linear dependent endmember spectra and consequently to strange abundances for the crop type endmembers that allow only a very limited comparison with the abundances of the proposed method.
   The classification with the highest abundance in a pixel ends up in an OA of 23.4% in the best case. Only *rapeseed* has good (over 90%) and *meadow young* and *winter barley* a trend to better (over 55%) PA and UA at once.

The main research question is:
Is it possible to capture the endmember variation of crop plants in an early stage of development for a mixture analysis by the proposed method?
This question can be answered based on the subordinate research questions with 'partially yes'. The spectral variation of *rapeseed* and at least a fraction of the spectral variation of *bare soil*, *bare soil bright* and *meadow young* can be captured. It is not possible to reliably distinguish *alfalfa* from *meadow*. For *meadow*, *spring barley*, *sugar pea*, *winter barley* and *winter wheat* a classification is only partially possible and therefore an exhaustive statement to the spectral differences to the other crop types cannot be made.

Exact abundances cannot be achieved by an analysis of the mixture with the proposed method, but it allows a statement about the membership of a crop type in a pixel. Due to missing data for validation this statement bases more upon assumptions and evidence in the literature (Atkinson and Lewis, 2000; Villa et al., 2011).

6.1. Outlook

A main problem of this thesis is the time gap between IS data acquisition and ground truth that complicates the assignment of the right crop type. Therefore, fieldwork and data acquisition at the same time would increase the reliability of the analysis. Especially for a spectral endmember library of vegetation signatures, which is necessary for a LSU, with an imaging spectrometer a synchronous measurement with the acquisition of IS data is required (Xie et al., 2008).

A further issue in this thesis and generally for SMA is the validation of the results (Keshava and Mustard, 2002). UAV are a possibility to get images with higher spatial resolution than the IS data, which allows to determine the mixture of a pixel more accurate for a validation. This need not be necessarily IS data for classification by hand; a true color image would be adequate.

There are several possibilities to improve the proposed method:

- Here the mean of the ROIs is used for the determination of the representative spectrum for each crop type, which requires adequate training data. One possibility to get a more representative spectrum is the application of the initially proposed method with the variogram cloud.
- The calculation of the threshold values based on the variogram is complex. The other approach already mentioned is to use statistical parameters for which standardized functions are available.
- To test the robustness of the proposed method the application to another test site would be interesting.

Appendix

Bibliography

Adams, J. B., Smith, M. O., Johnson, P. E., 1986. Spectral mixture modeling: A new analysis of rock and soil types at the Viking Lander 1 Site. Journal of Geophysical Research: Solid Earth 91 (B8), 8098–8112.

Atkinson, P. M., Lewis, P., 2000. Geostatistical classification for remote sensing: an introduction. Computers & Geosciences 26 (4), 361–371.

Bannari, A., Pacheco, A., Staenz, K., McNairn, H., Omari, K., 2006. Estimating and mapping crop residues cover on agricultural lands using hyperspectral and IKONOS data. Remote Sensing of Environment 104 (4), 447–459.

Bauer, M. E., Cipra, J. E., 1973. Identification of Agricultural Crops by Computer Processing of ERTS MSS Data. LARS Technical Reports Paper 20.
URL `http://docs.lib.purdue.edu/larstech/20`

Bioucas-Dias, J. M., Plaza, A., 2010. Hyperspectral Unmixing: Geometrical, Statistical, and Sparse Regression-Based Approaches. Image and Signal Processing for Remote Sensing XVI 5, 354–379.

Bioucas-Dias, J. M., Plaza, A., Camps-Valls, G., Scheunders, P., Nasrabadi, N., Chanussot, J., 2013. Hyperspectral Remote Sensing Data Analysis and Future Challenges. Geoscience and Remote Sensing Magazine, IEEE 1 (2), 6–36.

Bioucas-Dias, J. M., Plaza, A., Dobigeon, N., Parente, M., Du, Q., Gader, P., Chanussot, J., 2012. Hyperspectral Unmixing Overview: Geometrical, Statistical, and Sparse Regression-Based Approaches. IEEE Journal of Selected Topics in Applied Earth Observations and Remote Sensing 5 (2), 354–379.

Boardman, J., Kruse, F., Green, R., 1995. Mapping target signatures via partial unmixing of AVIRIS data. Summaries, Fifth JPL Airborne Earth Science Workshop JPL Public, 23–26.

Boardman, J. W., 1989. Inversion Of Imaging Spectrometry Data Using Singular Value Decomposition. In: Geoscience and Remote Sensing Symposium, 1989. IGARSS'89. Vol. 4. pp. 2069–2072.

Boardman, J. W., 1993. Automating spectral unmixing of AVIRIS data using convex geometry concepts. Summaries of the Fourth Annual JPL Airborne Geoscience Workshop, JPL Pub. 93-26, AVIRIS Workshop. 1, 11–14.

Chang, C.-I., Wang, S., 2006. Constrained band selection for hyperspectral imagery. IEEE Transactions on Geoscience and Remote Sensing 44 (6), 1575–1585.

Chilès, J.-P., Delfiner, P., 2012. Geostatistics: modeling spatial uncertainty, 2nd Edition. Hoboken: Wiley.

Clark, R. N., Roush, T. L., 1984. Reflectance spectroscopy: Quantitative analysis techniques for remote sensing applications. Journal of Geophysical Research: Solid Earth 89 (B7), 6329–6340.

Cohen, J., 1960. A Coefficient of Agreement for Nominal Scales. Educational and Psychological Measurement 20 (1), 37–46.

Craig, M. D., 1994. Minimum-volume transforms for remotely sensed data. IEEE Transactions on Geoscience and Remote Sensing 32 (3), 542–552.

Crookston, R. K., 2006. A Top 10 List of Developments and Issues Impacting Crop Management and Ecology During the Past 50 Years. Crop Science 46, 2253–2262.

Curran, P. J., Atkinson, P. M., 1998. Geostatistics and remote sensing. Progress in Physical Geography 22 (1), 61–78.

De Wit, a. J. W., Clevers, J. G. P. W., 2004. Efficiency and accuracy of per-field classification for operational crop mapping. International Journal of Remote Sensing 25 (20), 4091–4112.

Defries, R. S., Townshend, J. R. G., 1999. Global land cover characterization from satellite data: from research to operational implementation? Global Ecology and Biogeography 8 (5), 367–379.

Foerster, S., Kaden, K., Foerster, M., Itzerott, S., 2012. Crop type mapping using spectral-temporal profiles and phenological information. Computers and Electronics in Agriculture 89, 30–40.

Garrigues, S., Allard, D., Baret, F., 2008a. Modeling temporal changes in surface spatial heterogeneity over an agricultural site. Remote Sensing of Environment 112 (2), 588–602.

Garrigues, S., Allard, D., Baret, F., Morisette, J., 2008b. Multivariate quantification of landscape spatial heterogeneity using variogram models. Remote Sensing of Environment 112 (1), 216–230.

Green, A. A., Berman, M., Switzer, P., Craig, M. D., 1988. A transformation for ordering multispectral data in terms of image quality with implications for noise removal. IEEE Transactions on Geoscience and Remote Sensing 26 (1), 65–74.

Hengl, T., 2006. Finding the right pixel size. Computers & Geosciences 32 (9), 1283–1298.

Hudson, W. D., Ramm, C. W., 1987. Correct formulation of the kappa-coefficient of agreement. Photogrammetric engineering and remote sensing 53 (4), 421.

Hueni, A., Lenhard, K., Baumgartner, A., Schaepman, M. E., 2013. Airborne Prism Experiment Calibration Information System. IEEE Transactions on Geoscience and Remote Sensing 51 (11), 5169–5180.

Iordache, M.-d. M.-D., Bioucas-dias, J. M., Plaza, A., Member, S., 2011. Sparse Unmixing of Hyperspectral Data. IEEE Transactions on Geoscience and Remote Sensing 49 (6), 2014–2039.

Jewell, N., 1989. An evaluation of multi-date SPOT data for agriculture and land use mapping in the United Kingdom. International Journal of Remote Sensing 10 (6), 939–951.

Jolliffe, I., 2005. Principal component analysis. Encyclopedia of Statistics in Behavioral Science 3, 1580–1584.

Jupp, D. L. B., Strahler, A. H., Woodcock, C. E., 1988. Autocorrelation and regularization in digital images. I. Basic theory. IEEE Transactions on Geoscience and Remote Sensing 26 (4), 463–473.

Keshava, N., Mustard, J. F., 2002. Spectral unmixing. IEEE Signal Processing Magazine 19 (1), 44–57.

Lancashire, P. D., Bleiholder, H., van der Boom, T., Langelüddeke, P., Stauss, R., Weber, E., Witzenberger, A., 1991. A uniform decimal code for growth stages of crops and weeds. Annals of Applied Biology 119 (3), 561–601.

Landis, J. R., Koch, G. G., 1977. The Measurement of Observer Agreement for Categorical Data. Biometrics 33 (1), 159–174.

Lee, J. B., Woodyatt, A. S., Berman, M., 1990. Enhancement of high spectral resolution remote-sensing data by a noise-adjusted principal components transform. IEEE Transactions on Geoscience and Remote Sensing 28 (3), 295–304.

Li, L., Zhang, L., Zhang, F., 2013. Crop Mixtures and the Mechanisms of Overyielding. Encyclopedia of Biodiversity, 382–395.

MeteoSchweiz, 2013a. Klimabulletin Frühling 2013. Tech. rep., Zürich, Schweiz.

MeteoSchweiz, 2013b. Klimabulletin Mai 2013. Tech. rep., Zürich, Schweiz.

Mulla, D. J., 2013. Twenty five years of remote sensing in precision agriculture: Key advances and remaining knowledge gaps. Biosystems Engineering 114 (4), 358–371.

Mustard, J. F., 1993. Relationships of soil, grass, and bedrock over the kaweah serpentinite melange through spectral mixture analysis of AVIRIS data. Remote Sensing of Environment 44 (2-3), 293–308.

Nachtegael, M., Van der Weken, D., Kerre, E. E., Philips, W. (Eds.), 2007. Soft Computing in Image Processing. Springer, Berlin Heidelberg.

Nascimento, J. M. P., Bioucas-Dias, J. M., 2005. Vertex component analysis: A fast algorithm to unmix hyperspectral data. IEEE Transactions on Geoscience and Remote Sensing 43 (4), 898–910.

Olshausen, B. A., Field, D. J., 1996. Emergence of simple-cell receptive field properties by learning a sparse code for natural images. Nature 381, 607–609.

Pacheco, A., McNairn, H., 2010. Evaluating multispectral remote sensing and spectral unmixing analysis for crop residue mapping. Remote Sensing of Environment 114 (10), 2219–2228.

Panigrahy, S., Chakraborty, M., 1998. An integrated approach for potato crop intensification using temporal remote sensing data. ISPRS Journal of Photogrammetry and Remote Sensing 53 (1), 54–60.

Pebesma, E. J., 2004. Multivariable geostatistics in S: the gstat package. Computers & Geosciences 30, 683–691.

Peddle, D. R., Smith, A. M., 2005. Spectral mixture analysis of agricultural crops: Endmember validation and biophysical estimation in potato plots. International Journal of Remote Sensing 26 (22), 4959–4979.

Plaza, A., Martinez, P., Perez, R., Plaza, J., 2004. A quantitative and comparative analysis of endmember extraction algorithms from hyperspectral data. IEEE Transactions on Geoscience and Remote Sensing 42 (3), 650–663.

Richards, J. A., Xiuping, J., 1999. Remote Sensing Digital Image Analysis: An Introduction. Springer-Verlag, Berlin, Germany.

Roberts, D., Smith, M., Adams, J., 1993. Green vegetation, nonphotosynthetic vegetation, and soils in AVIRIS data. Remote Sensing of Environment 44 (2-3), 255–269.

Schaepman, M. E., Jehle, M., Hueni, A., D'Odorico, P., Damm, A., Weyermann, J., Schneier, F. D., Laurent, V., Popp, C., Seidel, F. C., Lenhard, K., Gege, P., Küchler, C., Brazile, J., Kohler, P., de Vos, L., Meulemann, K., Meynart, R., Schläpfer, D., Itten, K. I., submitted. Advanced radiometry measurements and Earth science applications with the Airborne Prism Experiment (APEX). Remote Sensing of Environment.

Scharf, L. L., 1991. The SVD and reduced rank signal processing. Signal Processing 25 (2), 113–133.

Schowengerdt, R., 1996. On the estimation of spatial-spectral mixing with classifier likelihood functions. Pattern Recognition Letters 17 (13), 1379–1387.

Somers, B., Asner, G. P., Tits, L., Coppin, P., 2011. Endmember variability in Spectral Mixture Analysis: A review. Remote Sensing of Environment 115 (7), 1603–1616.

Torres-Sánchez, J., Peña, J., de Castro, A., López-Granados, F., 2014. Multi-temporal mapping of the vegetation fraction in early-season wheat fields using images from UAV. Computers and Electronics in Agriculture 103, 104–113.

Van der Meer, F., 1999. Iterative spectral unmixing (ISU). International Journal of Remote Sensing 20 (17), 3431–3436.

Van der Meer, F., 2012. Remote-sensing image analysis and geostatistics. International Journal of Remote Sensing 33 (18), 5644–5676.

Villa, A., Chanussot, J., Benediktsson, J. A., Jutten, C., 2011. Spectral Unmixing for the Classification of Hyperspectral Images at a Finer Spatial Resolution. IEEE Journal of Selected Topics in Signal Processing 5 (3), 521–533.

Wang, C., Menenti, M., Stoll, M.-P., Belluco, E., Marani, M., 2007. Mapping mixed vegetation communities in salt marshes using airborne spectral data. Remote Sensing of Environment 107 (4), 559–570.

Winter, M. E., 1999. N-FINDR: an algorithm for fast autonomous spectral end-member determination in hyperspectral data. In: Imaging Spectrometry V. Vol. 3753. Proc. SPIE, pp. 266–275.

Woodcock, C. E., Strahler, A. H., Jupp, D. L. B., 1988. The use of variograms in remote sensing: I. Scene models and simulated images. Remote Sensing of Environment 25 (3), 323–348.

Xie, Y., Sha, Z., Yu, M., 2008. Remote sensing imagery in vegetation mapping: a review. Journal of Plant Ecology 1 (1), 9–23.

Nomenclature

ANC Abundance Nonnegativity Constraint

APEX Airborne Prism EXperiment

ASC Abundance Sum-to-one Constraint

BBCH Biologische Bundesanstalt, Bundessortenamt und CHemische Industrie

Exp Exponential model

IS Imaging Spectroscopy

LMM Linear Mixing Model

LSU Linear Spectral Unmixing

MNF Minimum Noise Fraction

MV Minimum Volume

NA Not Applicable value in R

NAPC Noise Adjusted Principle Components

NDVI Normalized Difference Vegetation Index

OA Overall Accuracy

PA Producer Accuracy

PCA Principal Component Analysis

PPI Pixel Purity Index

RMS Root-Mean-Square

RMSE Root-Mean-Square Error

ROI Region Of Interest

SMA Spectral Mixture Analysis

SNR Signal-to-Noise-Ratio

Sph Spherical model

SVD Singular Value Decomposition

SWIR Short-Wavelength InfraRed

UA User Accuracy

UAV Unmanned Aerial Vehicles

VNIR Visible and Near-InfraRed

A. PCA Band Selection

10 fields are randomly selected (Figure A.1). APEX bands 1-3 and 254-299 are left out, because they created problems in MNF-transformation. Therefore a spectral range from 413.6 nm to 2201.8 nm is used (Figure A.2). Based on the eigenvalue criterion (see section 3.2.1) PCA band subsets are formed. Differences between the APEX spectrum and the transformed and inverse transformed PCA band subsets can be seen in Figure A.3. The differences are all smaller than 2% for the mean over all 10 fields. For the selected PCA band subset (band 1-7) the largest difference between the mean of the original spectra and inverse transformed PCA spectra can be found in a pixel of a meadow field (Figure A.4). The largest deviations in the spectra can be found in the steep parts of the curve.

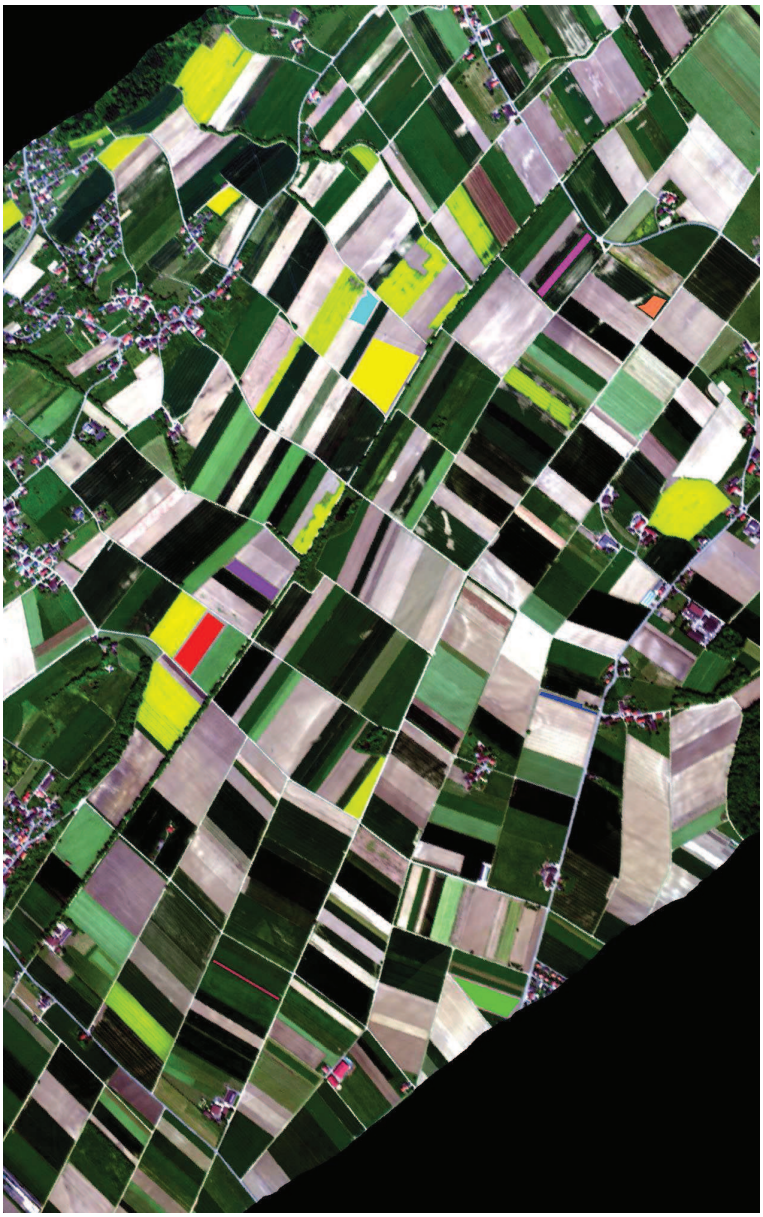

crop type	color
bare soil	red
bare soil	green
bare soil	blue
bare soil bright	yellow
bare soil bright	cyan
meadow	magenta
meadow	maroon
spring barley	sea green
spring barley	purple
winter barley	coral

Figure A.1.: Randomly selected fields for validation of the principal component analysis transformation.

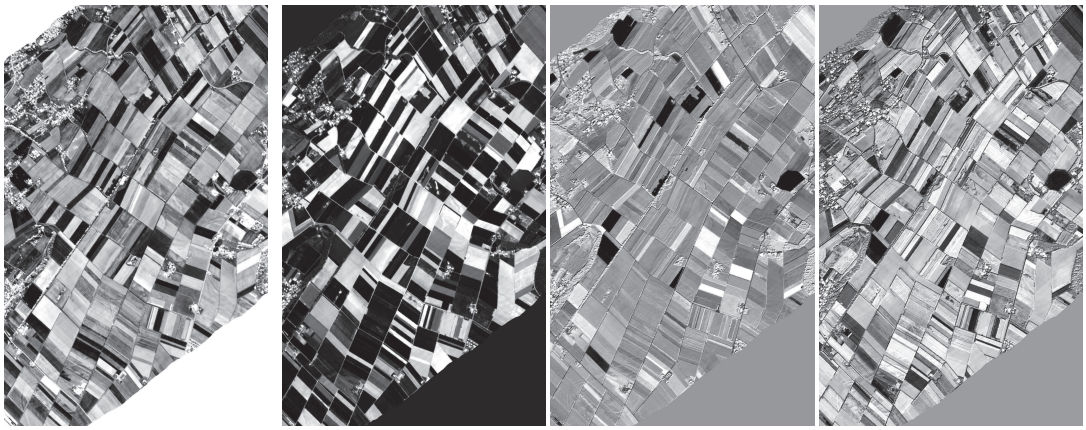

(a) PCA band 1 (b) PCA band 2 (c) PCA band 3 (d) PCA band 4

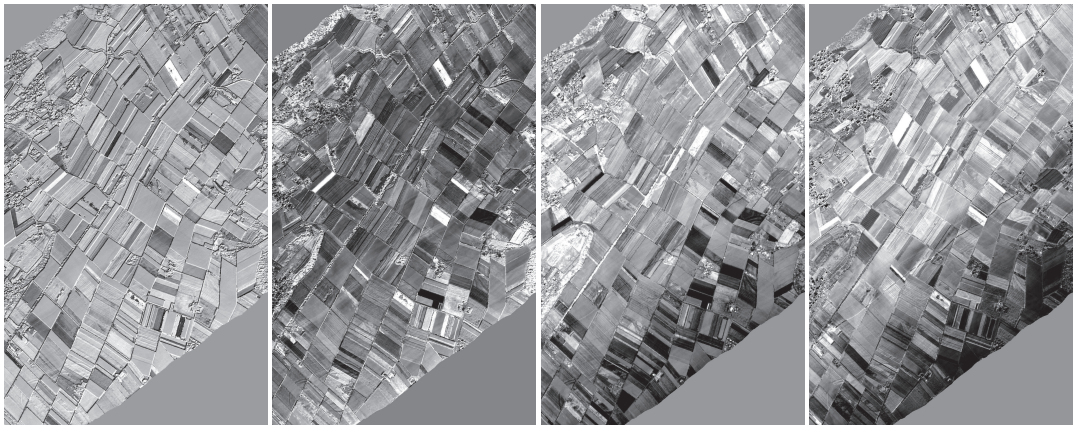

(e) PCA band 5 (f) PCA band 6 (g) PCA band 7 (h) PCA band 8

Figure A.2.: PCA transformed APEX bands 4-253.

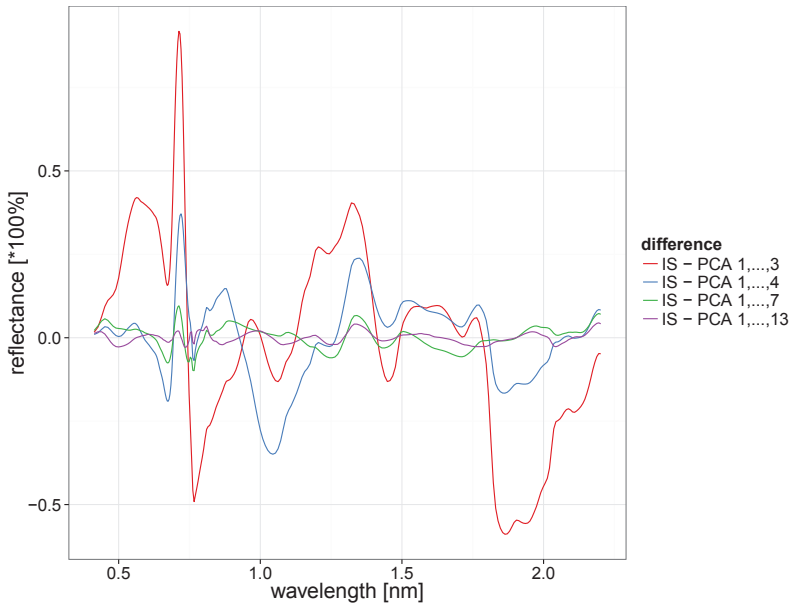

Figure A.3.: Comparison IS data (original APEX data) with transformed and inverse transformed PCA band subsets. Difference between the mean of the original and PCA band subset.

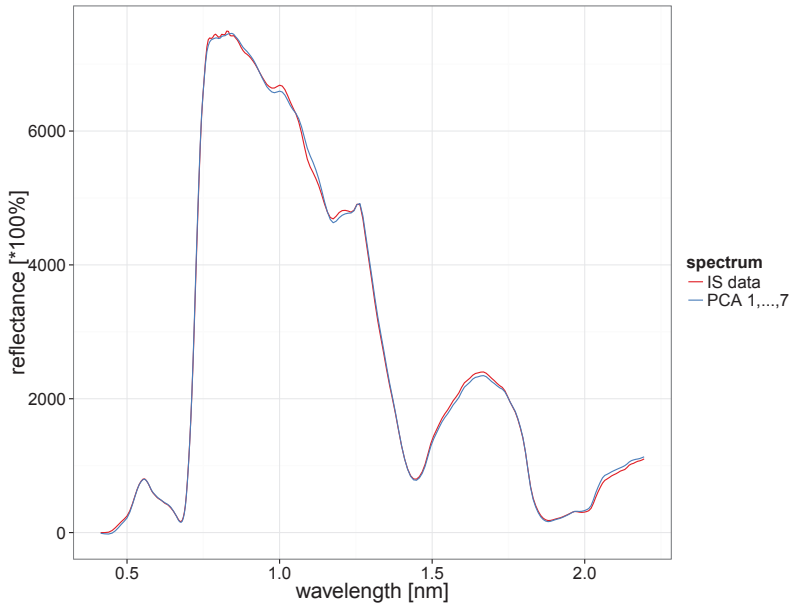

(a)

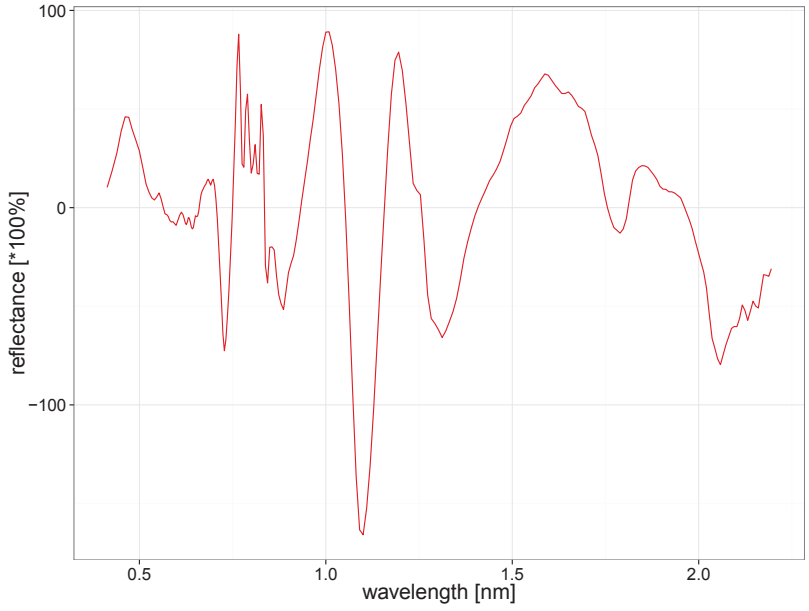

(b)

Figure A.4.: Pixel with biggest difference between APEX spectra and inverse transformed PCA spectra: spectra (a) and difference (b).

B. Additional Results

B.1. Proposed Method

B.1.1. Abundance

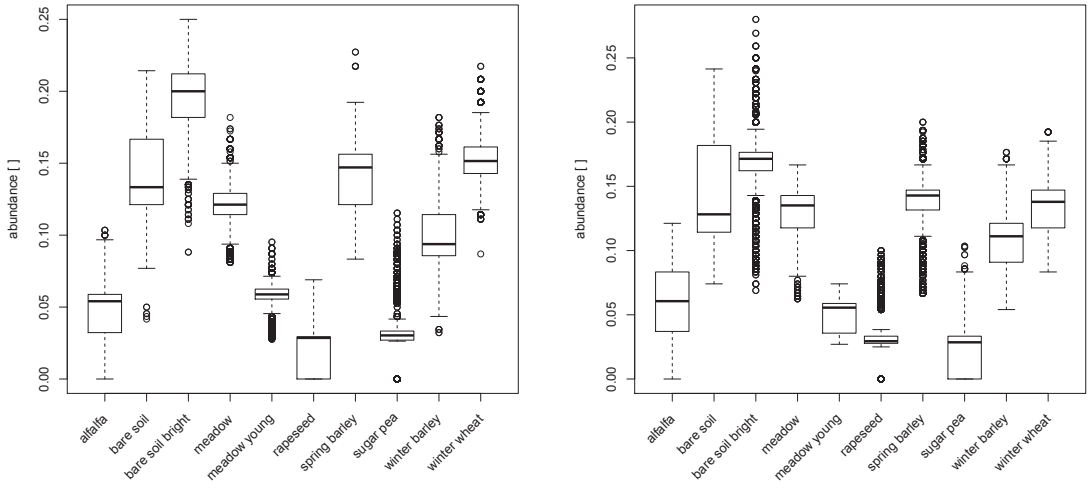

(a) (b)

Figure B.1.: Box plots of the abundances of the two neighboring fields of the *sugar pea* field. *Bare soil bright* field in the northwest (a) and *bare soil* field in the southeast (b).

B.1.2. Classification

Table B.1.: Producer accuracy (PA) and user accuracy (UA) for modal filtered simple classifications of first four window sizes and window size of maximum overall accuracy. NA values occur where no pixels are classified as the corresponding crop type.

modal filter size	1		3		5		7		23	
	PA [%]	UA [%]	PA [%]	UA [%]	PA [%]	UA [%]	PA [%]	UA [%]	PA [%]	UA [%]
alfalfa	0.00	0.00	0.00	0.00	0.00	NA	0.00	NA	0.00	NA
bare soil	51.37	81.76	53.73	84.89	54.97	86.22	55.74	86.97	57.31	88.35
bare soil bright	55.14	64.50	58.53	67.08	60.50	68.75	61.84	69.57	67.31	73.16
meadow	54.90	39.25	59.29	42.85	61.18	44.80	62.07	45.86	66.32	47.66
meadow young	96.27	55.80	98.40	56.29	99.27	57.02	99.42	57.56	99.69	59.82
rapeseed	62.15	97.62	68.56	99.01	72.09	99.23	73.58	99.34	79.88	100.00
spring barley	35.16	17.64	39.88	19.87	43.08	21.15	44.93	21.91	44.10	21.70
sugar pea	6.68	64.11	5.99	88.89	4.69	100.00	2.39	100.00	0.00	NA
winter barley	52.10	13.44	58.56	14.64	62.16	15.26	64.75	15.62	74.36	17.34
winter wheat	22.53	53.69	22.18	60.74	21.50	64.42	20.80	66.63	16.22	69.10
overall accuracy [%]	47.90		50.62		51.98		52.69		54.24	
kappa	0.07374		0.07815		0.08036		0.08151		0.08404	

Table B.2.: Producer accuracy (PA) and user accuracy (UA) for modal filtered advanced of first four window sizes and window size of maximum overall accuracy classifications. NA values occur where no pixels are classified as the corresponding crop type.

modal filter size	1		3		5		7		19	
	PA [%]	UA [%]	PA [%]	UA [%]	PA [%]	UA [%]	PA [%]	UA [%]	PA [%]	UA [%]
alfalfa	0.00	NA	0.00	NA	0.00	NA	0.00	NA	0.00	NA
bare soil	43.79	87.44	53.65	85.80	56.54	86.49	58.01	86.95	59.68	87.81
bare soil bright	46.05	68.98	57.17	68.12	60.38	69.43	61.98	70.23	65.92	72.52
meadow	45.40	52.47	59.19	47.52	61.58	47.53	62.52	47.82	65.10	48.48
meadow young	94.74	61.27	98.55	56.81	99.42	56.92	99.62	57.21	99.99	57.95
rapeseed	54.23	99.28	71.02	98.74	74.33	98.58	76.09	98.81	81.41	99.00
spring barley	25.01	22.66	40.36	22.69	42.99	22.82	44.31	23.05	42.85	22.51
sugar pea	4.79	98.97	7.33	100.00	6.18	100.00	3.24	100.00	0.00	NA
winter barley	43.36	15.96	61.14	15.71	66.56	16.05	69.31	16.23	75.15	16.84
winter wheat	13.36	76.96	20.90	72.64	21.00	71.94	20.43	71.42	16.28	69.16
unclassified	NA	0.00	NA	0.00	NA	0.00	NA	0.00	NA	0.00
overall accuracy [%]	39.66		50.33		52.57		53.50		54.45	
kappa	0.06145		0.07789		0.08137		0.08284		0.08437	

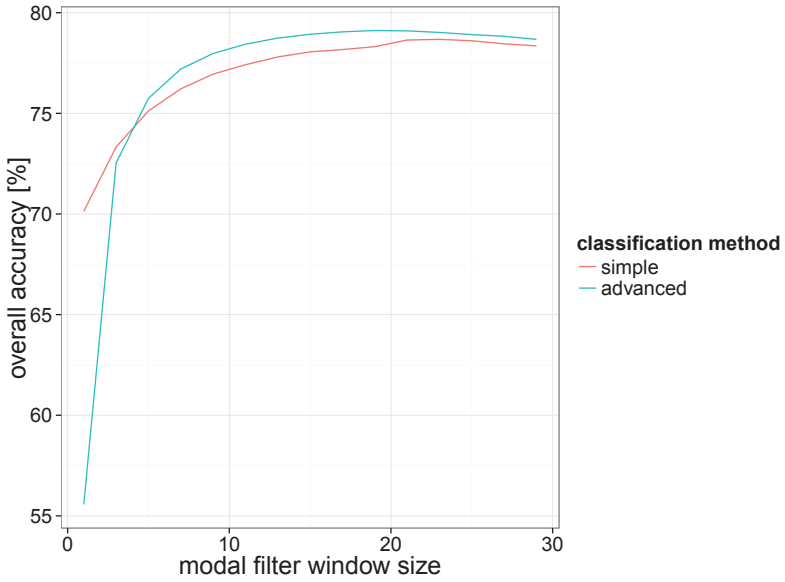

Figure B.2.: Overall accuracy for merged crop types and modal filter window size.

B.2. Confidence matrices

Table B.3.: Confidence matrix of simple classification of proposed method and modal filter window of size 1. Overall accuracy = 47.90%, kappa = 0.07374

classification	reference data													user accuracy [%]
	alfalfa	bare soil	bare soil bright	meadow	meadow young	rapeseed	spring barley	sugar pea	winter barley	winter wheat	unclassified	total		
alfalfa	0	0	0	191	0	5	27	0	1	5	0	229		0.00
bare soil	0	37264	5019	13	0	0	704	1080	93	1405	0	45578		81.76
bare soil bright	0	13524	31011	118	10	18	226	3	1653	1517	0	48080		64.50
meadow	1280	10218	1629	19186	219	1270	4796	698	1041	8544	0	48881		39.25
meadow young	0	208	19	3319	17291	3332	5599	0	0	1217	0	30985		55.80
rapeseed	0	95	0	52	69	9492	0	0	0	15	0	9723		97.62
spring barley	7	5818	5301	4764	237	998	8319	1	1626	20102	0	47173		17.64
sugar pea	0	34	2	0	5	8	17	134	0	9	0	209		64.11
winter barley	164	1091	9175	5531	82	143	2705	0	5314	15330	0	39535		13.44
winter wheat	44	4289	4087	1772	48	7	1269	89	472	14001	0	26078		53.69
unclassified	0	0	0	0	0	0	0	0	0	0	0	0		NA
total	1495	72541	56243	34946	17961	15273	23662	2005	10200	62145	0	296471		
producer accuracy [%]	0.00	51.37	55.14	54.90	96.27	62.15	35.16	6.68	52.10	22.53	NA			

Table B.4.: Confidence matrix of advanced classification of proposed method and modal filter window of size 23. Overall accuracy = 54.24%, kappa = 0.08404

classification	reference data									
	alfalfa	bare soil	bare soil bright	meadow	meadow young	rapeseed	spring barley	sugar pea	winter barley	winter wheat	unclassified	total	user accuracy [%]
alfalfa	0	0	0	0	0	0	0	0	0	0	0	0	NA
bare soil	0	41573	4123	11	0	8	0	1263	74	5	0	47057	88.35
bare soil bright	0	12974	37858	0	0	12	0	0	762	138	0	51744	73.16
meadow	1495	12189	579	23175	0	1050	3048	742	741	5610	0	48629	47.66
meadow young	0	290	0	2712	17906	1879	6070	0	17	1061	0	29935	59.82
rapeseed	0	0	0	0	0	12200	0	0	0	0	0	12200	100.00
spring barley	0	2713	2925	6738	49	124	10434	0	872	24217	0	48072	21.70
sugar pea	0	0	0	0	0	0	0	0	0	0	0	0	NA
winter barley	0	249	9061	2051	6	0	3760	0	7585	21033	0	43745	17.34
winter wheat	0	2553	1697	259	0	0	0	0	0	10081	0	14590	69.10
unclassified	0	0	0	0	0	0	350	0	149	0	0	499	0.00
total	1495	72541	56243	34946	17961	15273	23662	2005	10200	62145	0	296471	
producer accuracy [%]	0.00	57.31	67.31	66.32	99.69	79.88	44.10	0.00	74.36	16.22	NA		

Table B.5.: Confidence matrix of advanced classification of proposed method and modal filter window of size 1. Overall accuracy = 39.66%, kappa = 0.06145

classification	reference data													user accuracy [%]
	alfalfa	bare soil	bare soil bright	meadow	meadow young	rapeseed	spring barley	sugar pea	winter barley	winter wheat	unclassified	total		
alfalfa	0	0	0	0	0	0	0	0	0	0	0	0		NA
bare soil	0	31769	3410	0	0	0	87	729	17	322	0	36334		87.44
bare soil bright	0	10496	25900	8	0	1	15	0	773	352	0	37545		68.98
meadow	1132	4114	272	15865	125	711	2729	380	856	4053	0	30237		52.47
meadow young	0	97	4	2463	17017	2166	5122	0	0	907	0	27776		61.27
rapeseed	0	51	0	0	7	8283	0	0	0	2	0	8343		99.28
spring barley	0	704	2446	2524	63	190	5919	0	638	13642	0	26126		22.66
sugar pea	0	0	1	0	0	0	0	96	0	0	0	97		98.97
winter barley	34	179	6814	2035	21	3	2113	0	4423	12089	0	27711		15.96
winter wheat	0	761	1080	292	3	0	278	0	73	8305	0	10792		76.96
unclassified	329	24370	16316	11759	725	3919	7399	800	3420	22473	0	91510		0.00
total	1495	72541	56243	34946	17961	15273	23662	2005	10200	62145	0	296471		
producer accuracy [%]	0.00	43.79	46.05	45.40	94.74	54.23	25.01	4.79	43.36	13.36	NA			

Table B.6.: Confidence matrix of advanced classification of proposed method and modal filter window of size 19. Overall accuracy = 54.45%, kappa = 0.08437

classification	reference data									
	alfalfa	bare soil	bare soil bright	meadow	meadow young	rapeseed	spring barley	sugar pea	winter barley	winter wheat	unclassified	total	user accuracy [%]
alfalfa	0	0	0	0	0	0	0	0	0	0	0	0	NA
bare soil	0	43294	4583	18	0	8	0	1250	74	77	0	49304	87.81
bare soil bright	0	13195	37078	1	0	6	0	0	672	174	0	51126	72.52
meadow	1495	10937	474	22750	0	1028	3001	755	792	5699	0	46931	48.48
meadow young	0	889	15	2856	17960	1777	6249	0	23	1222	0	30991	57.95
rapeseed	0	125	0	0	0	12433	0	0	0	0	0	12558	99.00
spring barley	0	1283	3046	6566	1	21	10138	0	871	23110	0	45036	22.51
sugar pea	0	0	0	0	0	0	0	0	0	0	0	0	NA
winter barley	0	499	9111	2498	0	0	3993	0	7665	21745	0	45511	16.84
winter wheat	0	2319	1936	257	0	0	0	0	0	10118	0	14630	69.16
unclassified	0	0	0	0	0	0	281	0	103	0	0	384	0.00
total	1495	72541	56243	34946	17961	15273	23662	2005	10200	62145	0	296471	
producer accuracy [%]	0.00	59.68	65.92	65.10	99.99	81.41	42.85	0.00	75.15	16.28	NA		

Table B.7.: Confidence matrix of advanced classification of constrained conventional approach and modal filter window of size 1. Overall accuracy = 5.93%, kappa = 0.00827

classification	reference data													
	alfalfa	bare soil	bare soil bright	meadow	meadow young	rapeseed	spring barley	sugar pea	winter barley	winter wheat	unclassified	total	user accuracy [%]
alfalfa	0	0	0	6400	0	0	5267	0	1197	17061	0	29925	0.00
bare soil	0	139	29	375	5386	4	204	0	1	494	0	6632	2.10
bare soil bright	0	0	0	2	0	113	0	0	0	81	0	196	0.00
meadow	0	4	4	2	1955	12124	0	0	0	5	0	14094	0.01
meadow young	607	0	0	7070	4275	2794	17	0	124	251	0	15138	28.24
rapeseed	0	14	11	1141	0	0	3	0	0	0	0	1169	0.00
spring barley	0	19396	9286	7545	0	0	1050	0	5848	18645	0	61770	1.70
sugar pea	0	52988	46913	170	0	0	1275	2005	2593	7086	0	113030	1.77
winter barley	888	0	0	10368	5859	65	12175	0	433	8848	0	38636	1.12
winter wheat	0	0	0	1873	486	173	3671	0	4	9674	0	15881	60.92
unclassified	0	0	0	0	0	0	0	0	0	0	0	0	NA
total	1495	72541	56243	34946	17961	15273	23662	2005	10200	62145	0	296471	
producer accuracy [%]	0.00	0.19	0.00	0.01	23.80	0.00	4.44	100.00	4.25	15.57	NA		

Table B.8.: Confidence matrix of advanced classification of unconstrained conventional approach and modal filter window of size 5. Overall accuracy = 23.4%, kappa = 0.0363

classification	reference data										
	alfalfa	bare soil	bare soil bright	meadow	meadow young	rapeseed	spring barley	sugar pea	winter barley	winter wheat	unclassified	total	user accuracy [%]
alfalfa	452	0	0	11896	0	0	509	0	652	4104	0	17613	2.57
bare soil	0	4604	409	5387	322	0	0	0	0	789	0	11511	40.00
bare soil bright	0	15130	11650	0	0	0	0	94	0	0	0	26874	43.35
meadow	0	0	0	512	0	0	530	0	2	557	0	1601	31.98
meadow young	0	7	0	1992	9977	0	15	0	0	1110	0	13101	76.15
rapeseed	0	0	1	0	0	14077	0	0	0	19	0	14097	99.86
spring barley	0	6870	4209	8548	4170	946	15656	0	978	13946	0	55323	28.30
sugar pea	1043	45930	39974	6457	3492	250	6689	1911	2598	33720	0	142064	1.35
winter barley	0	0	0	1	0	0	167	0	5964	3399	0	9531	62.57
winter wheat	0	0	0	153	0	0	46	0	0	4501	0	4700	95.77
unclassified	0	0	0	0	0	0	50	0	6	0	0	56	0.00
total	1495	72541	56243	34946	17961	15273	23662	2005	10200	62145	0	296471	
producer accuracy [%]	30.23	6.35	20.71	1.47	55.55	92.17	66.17	95.31	58.47	7.24	NA		

B.3. Box Plot of the PCA Bands

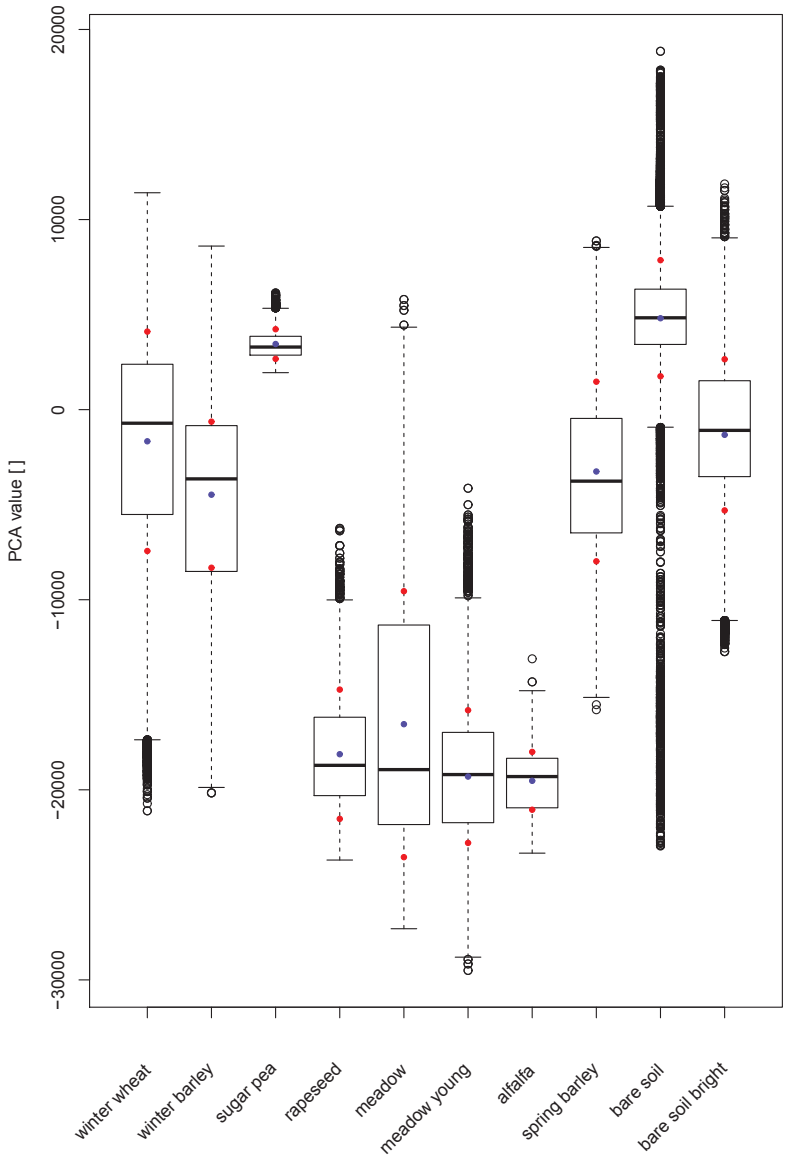

Figure B.3.: Box plot of the training data in PCA band 1. Whiskers are at 1.5 of the interquartile range and the outliers are marked with circles. Blue dots indicate the mean of crop type, red dots upper and lower threshold value.

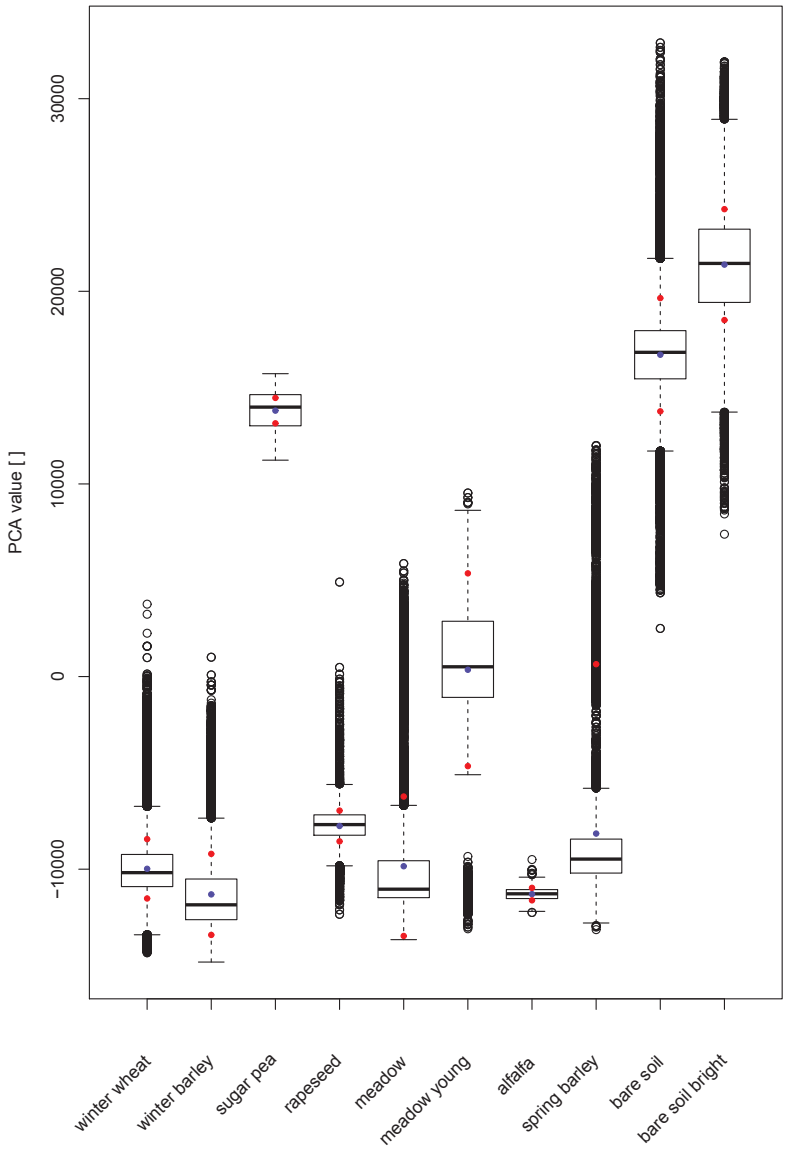

Figure B.4.: Box plot of the training data in PCA band 2. Whiskers are at 1.5 of the interquartile range and the outliers are marked with circles. Blue dots indicate the mean of crop type, red dots upper and lower threshold value.

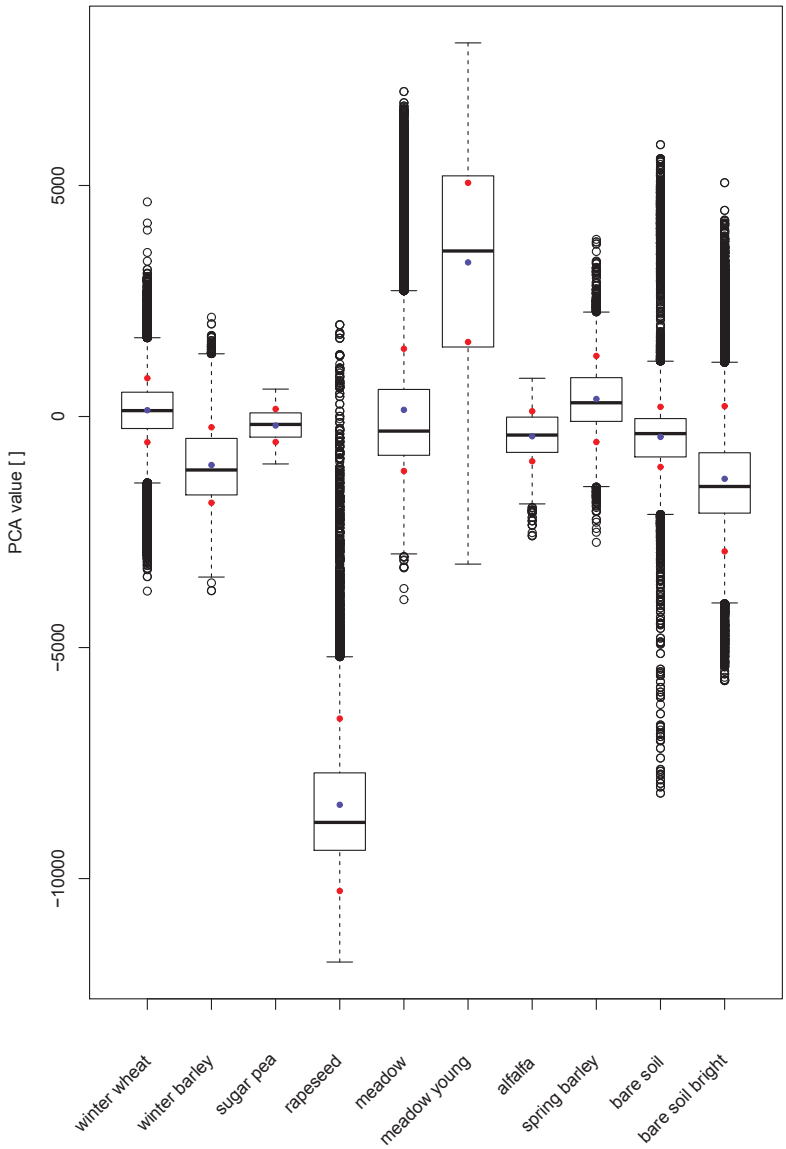

Figure B.5.: Box plot of the training data in PCA band 3. Whiskers are at 1.5 of the interquartile range and the outliers are marked with circles. Blue dots indicate the mean of crop type, red dots upper and lower threshold value.

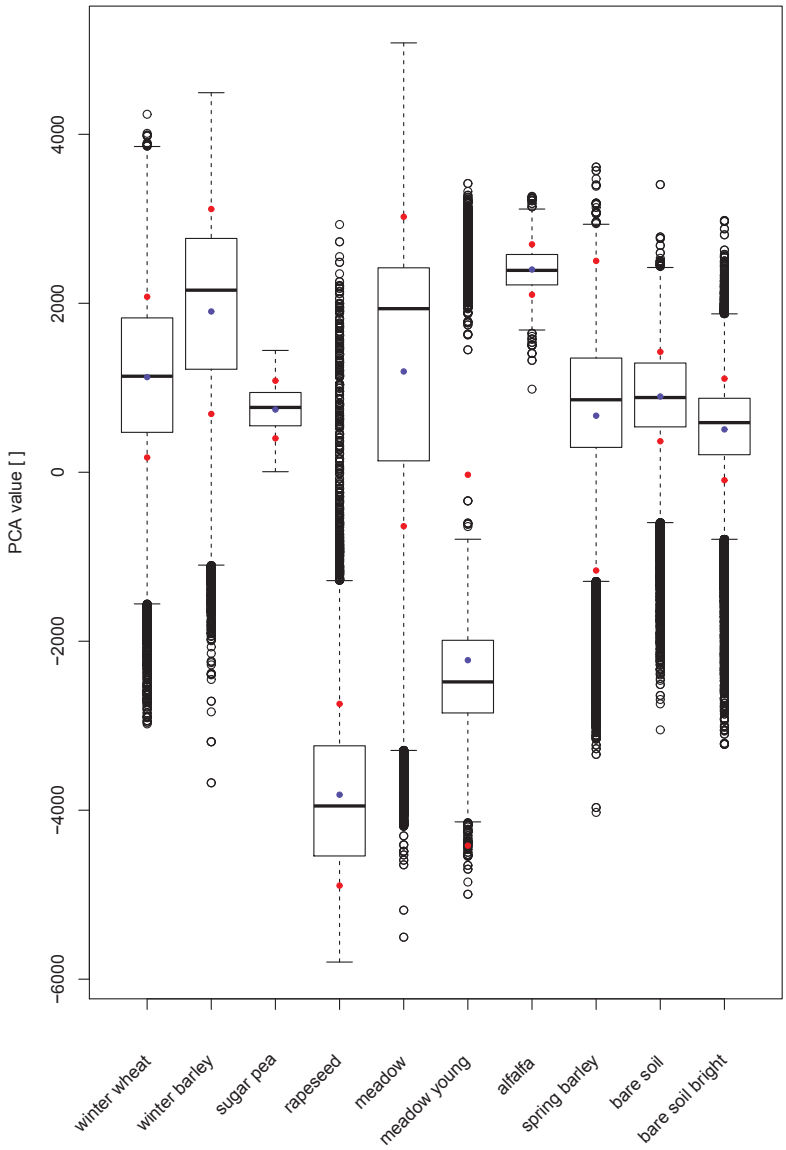

Figure B.6.: Box plot of the training data in PCA band 4. Whiskers are at 1.5 of the interquartile range and the outliers are marked with circles. Blue dots indicate the mean of crop type, red dots upper and lower threshold value.

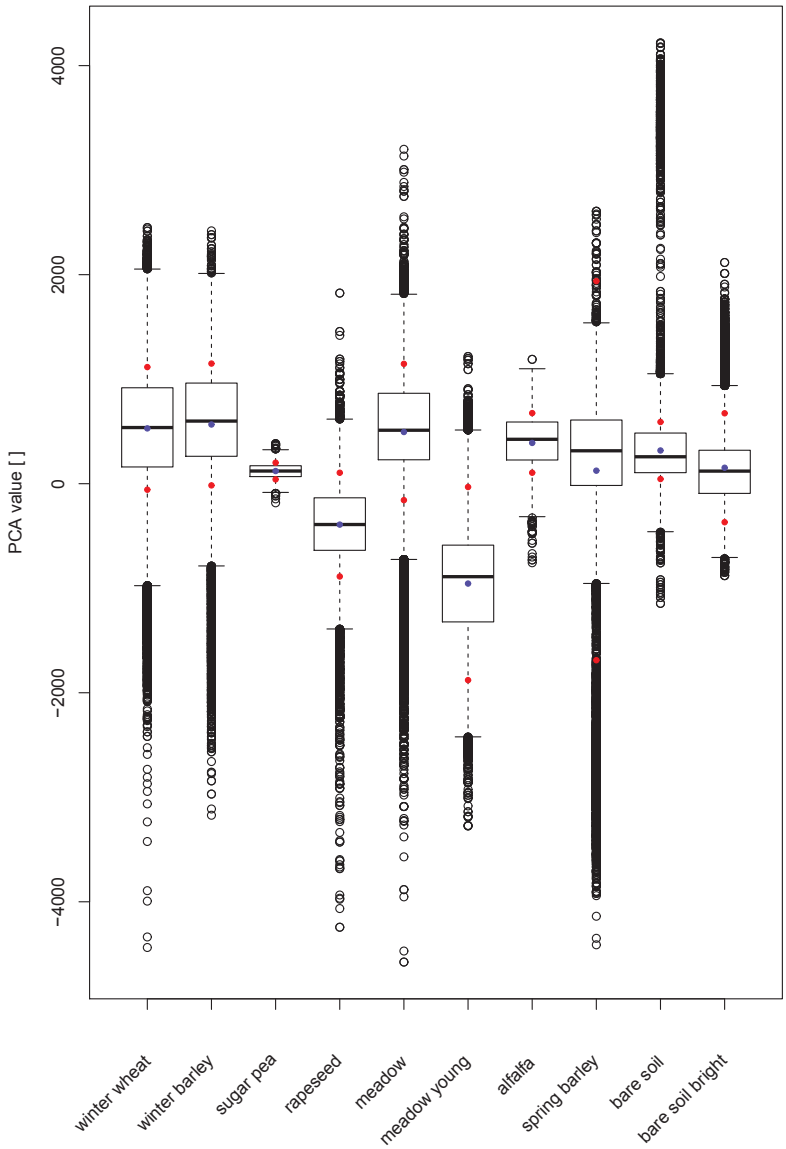

Figure B.7.: Box plot of the training data in PCA band 5. Whiskers are at 1.5 of the interquartile range and the outliers are marked with circles. Blue dots indicate the mean of crop type, red dots upper and lower threshold value.

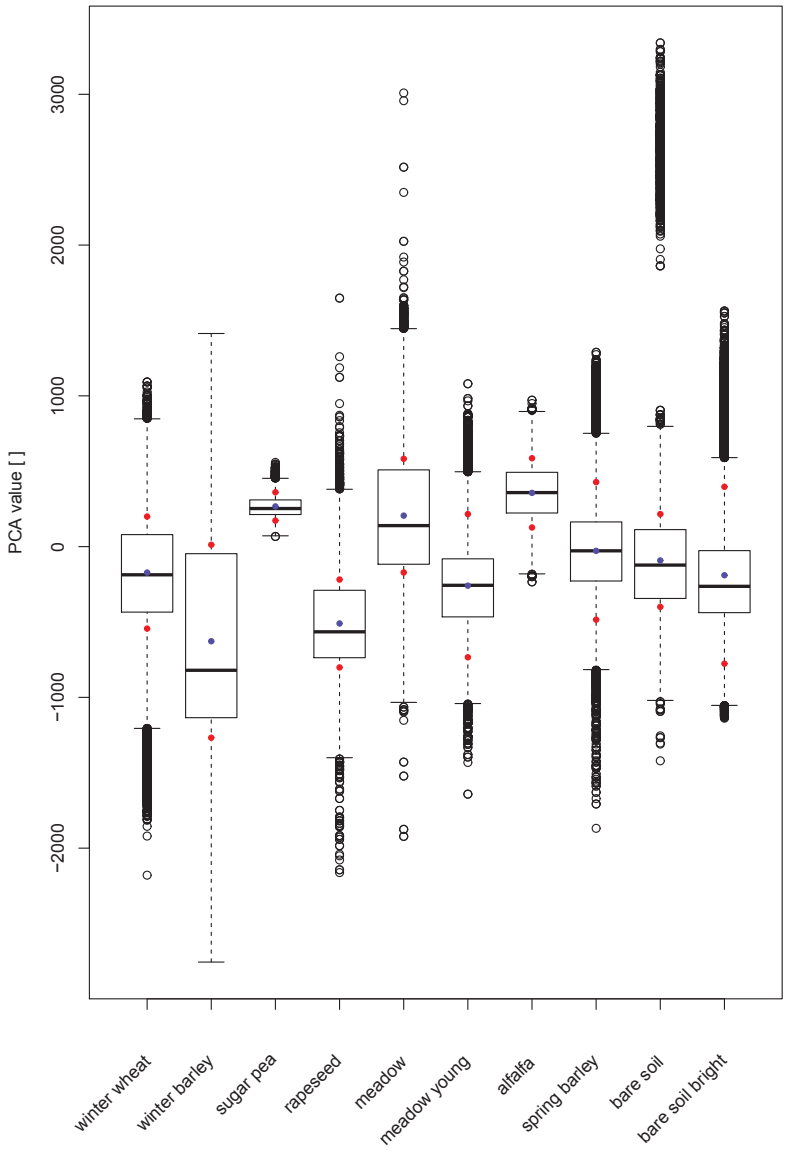

Figure B.8.: Box plot of the training data in PCA band 6. Whiskers are at 1.5 of the interquartile range and the outliers are marked with circles. Blue dots indicate the mean of crop type, red dots upper and lower threshold value.

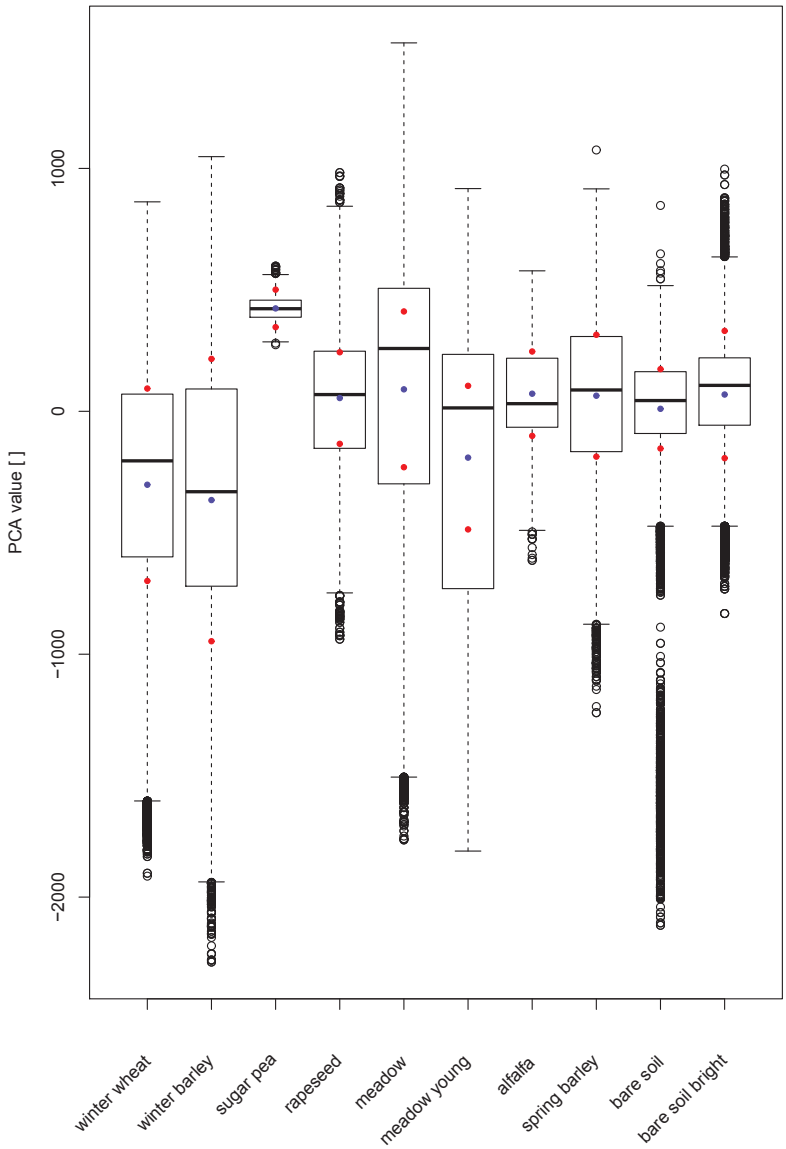

Figure B.9.: Box plot of the training data in PCA band 7. Whiskers are at 1.5 of the interquartile range and the outliers are marked with circles. Blue dots indicate the mean of crop type, red dots upper and lower threshold value.

B.4. Classification results of Foerster et al. (2012)

Table B.9.: UA and PA of 7 crop classes in the study of Foerster et al. (2012) that correspond to used crop types in the proposed method (modal filtered advanced classification with window of size 19).

study of Foerster et al. (2012)			proposed method		
labels	PA [%]	UA [%]	crop type	PA [%]	UA [%]
fallow	76.6	83.6	bare soil and bare soil bright	62.80	80.17
perennial field grass	0	0	meadow	65.10	48.48
winter wheat	91.7	76.8	winter wheat	16.28	69.16
winter barley	76.9	88.7	winter barley	75.15	16.84
oilseed rape	93.3	49.2	rapeseed	81.41	99.00
summer grain	0	0	partially spring barley	42.85	22.51
first year field grass	0	0	meadow young	99.99	57.95

Persönliche Erklärung

Persönliche Erklärung: Ich erkläre hiermit, dass ich die vorliegende Arbeit selbständig verfasst und die den verwendeten Quellen wörtlich oder inhaltlich entnommenen Stellen als solche kenntlich gemacht habe.

Winterthur, 30.4.2014